



Stefan Cesnik, BSc

The Role of Molecular Symmetries in Non-adiabatic Relaxation Dynamics

MASTER'S THESIS

to achieve the university degree of

Diplom-Ingenieur

Master's degree programme: Technical Physics

submitted to

Graz University of Technology

Supervisor:

Assoc.Prof.Dipl.-Ing.Dr. Markus Koch

Institute of Experimental Physics

Graz, May 2018

Affidavit

I declare that I have authored this thesis independently, that I have not used other than the declared sources/resources, and that I have explicitly indicated all material which has been quoted either literally or by content from the sources used. The text document uploaded to TUGRAZonline is identical to the present master's thesis.

Graz, _____

Date

Signature

Eidesstattliche Erklärung

Ich erkläre an Eides statt, dass ich die vorliegende Arbeit selbstständig verfasst, andere als die angegebenen Quellen/Hilfsmittel nicht benutzt, und die den benutzten Quellen wörtlich und inhaltlich entnommenen Stellen als solche kenntlich gemacht habe. Das in TUGRAZonline hochgeladene Textdokument ist mit der vorliegenden Diplomarbeit identisch

Graz, am _____

Datum

Unterschrift

Abstract

In this thesis isolated acetone molecules in gas phase were studied with femtosecond time-resolved photoelectron spectroscopy. The goal was the direct excitation of the low lying three 3p Rydberg states, namely the $3p_x$, $3p_y$ and $3p_z$. The pump-probe experiment was performed using two-photon excitation (333 nm pump wavelength) and one-photon ionization (400 nm probe wavelength). A time-of-flight (TOF) spectrometer in magnetic bottle configuration is used for detection of the kinetic energy of the electrons. The population dynamics of the 3p Rydberg states can be explained by internal conversion through coupling with valence states. Although acetone has been intensively studied, the state-resolved temporal behavior of the 3p Rydberg states has not been observed before. Every single 3p Rydberg state has a different symmetry, which allow new coupling rules with other states. The experiment is in cooperation with the theoretical group of Prof. Leticia Gonz  les from the University of Vienna, who performed simulations, indicating different time constants due to different symmetries of the respective 3p states.

Our existing pump-probe setup had to be extended to fulfill the following requirements: Tunable excitation wavelengths, increased energy resolution of the photoelectron spectra and an increased temporal resolution. The energy resolution was improved by modifying the TOF parameters. An optical parametric amplifier (OPA) and a prism compressor were installed into the pump path and characterized. An optimization procedure was developed to minimize the pulse-to-pulse fluctuations. The temporal resolution of the pump-probe setup was determined by measuring pump-probe cross-correlations with xenon gas.

Our result with a pump wavelength of 333 nm show good qualitative agreement with the theoretical calculations. As expected, the $3p_y$ decays the fastest with 400 fs compared to $3p_x$ and $3p_z$ (800 fs and 500 fs, respectively). Moreover, the well known effect of vibronic coupling was observed between the states, leading to population transfer, which is in good agreement with previous, non time-resolved studies.

Kurzfassung

Diese Arbeit präsentiert die zeitaufgelöste Photoelektronenspektroskopie mit Femtosekundenpulsen an isolierten Aceton Molekülen in Gasphase. Ziel war die direkte Anregung der niedrig liegenden 3p Rydberg Zustände, genauer des $3p_x$, $3p_y$ und $3p_z$. Das hier beschriebene Pump-Probe Experiment nutzt zwei Photonen (333 nm) zur Anregung und ein Photon (400 nm) zur Ionisation. Ein Flugzeitspektrometer (TOF) wurde zur Detektion der kinetischen Energie der Elektronen verwendet. Die Populationsdynamik der 3p Rydberg Zustände wird durch innere Konversion, durch Koppeln mit Valenzzuständen, erklärt. Obwohl Aceton in der Vergangenheit ausführlich untersucht wurde, ist es noch nicht gelungen, das zeitliche Verhalten der 3p Rydberg Zustände zustandsaufgelöst zu beobachten. Jeder einzelne dieser 3p Rydberg Zustände hat eine eigene Symmetrie, was neue Kopplungsregeln mit anderen Zuständen erlaubt. Das gesamte Experiment entstand in Zusammenarbeit mit der Theoriegruppe von Prof. Letizia Gonzáles (Universität Wien). Sie berechneten die Zeitkonstanten theoretisch und fanden heraus, dass sich diese aufgrund der verschiedenen Symmetrien der einzelnen 3p Zustände unterscheiden.

Der vorhandene experimentelle Aufbau musste erweitert werden, um folgende Bedingungen zu erfüllen: Durchstimbare Anregungswellenlängen, verbesserte Energieauflösung in den Photoelektronenspektren, sowie eine bessere zeitliche Auflösung. Hierzu wurden ein optisch parametrischer Verstärker (OPA) und ein Prismenkompressor in das Setup integriert. Die Energieauflösung konnte durch Modifikation der TOF Parameter gesteigert werden. Neben des Einbaus und der Charakterisierung des OPAs wurde auch eine Optimierungsroutine gefunden um Puls zu Puls Schwankungen zu minimieren. Mit Hilfe des optimierten Prismenkompressors konnte die zeitliche Auflösung durch Messungen der Pump-Probe-Kreuzkorrelation an Xenongas bestimmt werden.

Die Resultate zeigen eine qualitative Übereinstimmung mit den theoretischen Simulationen. Wie erwartet zerfällt der $3p_y$ am schnellsten mit 400 fs, verglichen mit $3p_x$ und $3p_z$ (jeweils 800 fs und 500 fs). Ebenfalls wurde der bekannte Effekt des vibronischen Koppels beobachtet, welcher zu Populationstransfers zwischen den 3p Zuständen führt.

Contents

1	Introduction	1
1.1	Time Resolved Photoelectron Spectroscopy	1
1.2	Symmetries	3
1.3	Acetone Literature	5
2	Experimental	9
2.1	Overview	9
2.1.1	Optical Setup	11
2.1.2	Parameters of SHG Crystals	13
2.1.3	TOF Energy Resolution	16
2.2	Optical Parametric Amplifier (OPA)	18
2.2.1	Basics	18
2.2.2	Working Principle and Power Optimization of our OPA	18
2.2.3	Stability of the OPA	23
2.2.4	OPA Security Box	24
2.3	How to Find and Shift Temporal Overlap	25
2.4	Prism Compressor	27
2.4.1	Adjusting the Prism Compressor in General	27
2.4.2	Improving the Temporal Resolution	29
2.5	Raspberry Pi	31
2.5.1	General Information about our Raspberry Pi	31
2.5.2	Starting the Raspberry Pi and some useful Commands	32
2.5.3	Adding New Sensors	32
2.5.4	New Server Certificate	35
3	Characterisation Measurements	37
3.1	Energy Resolution	38

3.2	Temporal Resolution	42
4	Results	47
4.1	3p Rydberg State Energies and Symmetries	48
4.2	Direct Excitation of the 3p _y Rydberg State	49
4.3	Evaluation of the PE Spectra	52
4.3.1	Measurement with >100 fs Temporal Resolution	52
4.3.2	Measurement with 77 fs Temporal Resolution	53
4.3.3	Vibronic Coupling of the 3p _x State	56
4.4	Summary, Outlook and Open Questions	57
5	Appendix	59
A	Raspberry Pi Hardware	59
B	Python Codes	62
B.1	simpletest.py	62
B.2	MCP3008.py	63
B.3	serial_test_class.py	64
B.4	pressure.py	65
C	OPA Wavelengths	67
D	Matlab Codes	67
D.1	pumpprobe_various_dt.m	68
D.2	create_eiTOFname.m	70
E	Detailed Measurement Routine	72
	Bibliography	76
	Danksagung	83

CHAPTER 1

Introduction

1.1 Time Resolved Photoelectron Spectroscopy

The observation of dynamical processes in molecules on ultra short time scales are made possible by using every shorter laser pulses. The interest is very high for this topic due to the fact that a lot of processes in nature take place at these short time scales. While nanosecond lasers are a conventional tool to measure band structures due to their energy resolution, information about the temporal behavior of the system can not be observed with them. By using shorter laser pulses of femtosecond pulse duration it became possible to obtain information of relaxation dynamics in a molecule.

A pioneer of using ultrashort laser pulses to study properties of molecules in femtochemistry was Ahmed Zewail who received the noble prize for chemistry in 1999 [1].

A detailed summary of femtosecond time resolved photoelectron spectroscopy can be found in the works of Stolow et al. [2] and Hertel and Radloff [3]. Pump-probe experiments using short pulses allow to track the dynamics of electrons and nuclei in a molecule in real time. Figure 1.1 demonstrates the general idea of such a configuration: A pump pulse (violet arrow) creates population in a resonant excited state (ES), followed by a time delayed (Δt) probe pulse (blue arrow), which allows to see the evolution of the population as a function of time. The probe pulse ionizes the molecule and furthermore, as detection method, the change of kinetic energy of electrons E_{kin} is used to understand the process above.

The kinetic energy of electrons can be calculated in the following way: In the most general

case the energies can be written as [3]

$$E_{\text{vo}} + h\nu_{\text{pump}} + h\nu_{\text{probe}} = E_{\text{kin}} + \text{IP} + E^+(\nu^+) \quad (1.1)$$

where E_{vo} is the internal energy of the system in the ground state, $h\nu_{\text{pump}}$, $h\nu_{\text{probe}}$ are the energies of pump and probe pulse, IP is the ionization potential, E_{kin} the kinetic energy of the electrons, and $E(\nu)$ are the energies of the vibrational levels with 'ES' for the excited- and '+' for the ionic state.

The term $E_{\text{vo}} + h\nu_{\text{pump}}$ can be rewritten as $E_{\text{vo}} + h\nu_{\text{pump}} = E_{\text{ES}} + E_{\text{ES}}(\nu)$ and included in equation 1.1:

$$E_{\text{ES}} + E_{\text{ES}}(\nu) + h\nu_{\text{probe}} = E_{\text{kin}} + \text{IP} + E^+(\nu^+) \quad (1.2)$$

Finally, the kinetic energy of the electrons can be calculated:

$$E_{\text{kin}} = E_{\text{ES}} + E_{\text{ES}}(\nu) + h\nu_{\text{probe}} - (\text{IP} + E^+(\nu^+)) \quad (1.3)$$

Formula 1.3 describes how the kinetic energy changes after electronic or vibrational relaxation of the excited state.

With the following experiment the time resolved spectroscopy of the 3p Rydberg states in acetone was performed. These states have some special character: The electronic states are parallel to each other. As consequence the transition between their vibrational levels is always given by $\Delta\nu=0$.

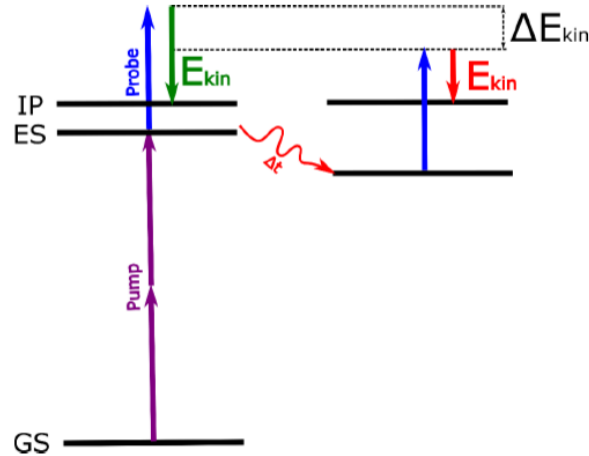


Figure 1.1: The basic principle for a pump-probe experiment.

The change of the kinetic energy can happen by three different mechanisms: internal conversion (IC), intersystem crossing (ISC) or internal vibrational energy redistribution (IVR). Internal conversion (IC) is a non radiative transition in a molecule where the

multiplicity does not change (same spin). The multiplicity of a quantum state is defined by: $M = 2S + 1$, with the spin quantum number S . States with $M = 1, 2, 3, 4, 5$ are called singlet, duplett, triplet state, quartett or quintett. In contrast, ISC is a transition where the spin changes. While IC and ISC are electronic relaxations, IVR describes vibrational relaxations.

Furthermore, non-adiabatic relaxation means that nuclear and electron motions can not be separated.

1.2 Symmetries

We meet symmetries every time in our daily life. They cover large fields of applications including physics, mathematics, architecture, chemistry or biology, just to show some examples. In general, if properties of a system do not change after applying certain operations (e.g. transition, rotation, reflection), namely symmetry operations, these properties are symmetry-invariant. The collection of all these operations is called symmetry group. A symmetry group contains symmetry elements. These are points, axis or planes which do not change their spatial location after applying symmetry operations. The symmetry group which describes all of these elements is called point group.

However, talking about symmetries makes only sense if we consider operations in coordination systems. Symmetries can be seen in different points of views depending on the studied system. In physics symmetries are often related to coordinate transformations and their conserved quantities (Noether Theorem), where the whole system does not change after transformations.

When talking about the shape of geometrical bodies, symmetries become better understandable. We will see on the example of acetone that symmetry considerations can be done in a classical way as geometry (C_{2v}) or, in contrast, in a quantum mechanic system electronic states can have different symmetries (A_1) too. Let us move on with a short excursion to the notation of symmetries: $C_{n\ v/h}$ indicates the rotation symmetry group C and describes that the symmetry after rotation of $\frac{360^\circ}{n}$ around the vertical (v) / horizontal (h) axis stays the same. There are some more symbols and groups, which can also be combined with each other:

- identity E
- inversion i
- rotation about axis C
- reflection through plane σ

- rotation followed by reflection through plane, which is perpendicular to rotation axis S

This master's thesis presents that the temporal behaviour of the population after photoexcitation of acetone in gas phase is going to be different, because of symmetry arguments. Symmetries in acetone can be discussed the following way: Figure 1.2 shows the chemical structure of acetone ($\text{C}_3\text{H}_6\text{O}$), having a C_{2v} symmetry. This means if the molecule is rotated by 180° around its vertical axis, it looks the same.

Furthermore, the electronic states have symmetries too, which can be imagined as the electron density distribution in the corresponding molecular orbital [4]. Both pictures are necessary to understand the deep processes inside of the molecule. Electronic transitions in acetone and how they are affected by symmetries are described in the next section.

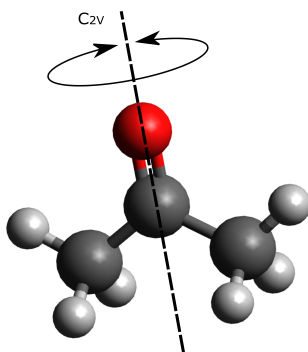


Figure 1.2: Sketch of acetone, showing the C_{2v} symmetry around the z-axis (dashed line).

The interpretation of the results was done with the help of a character table 1.1 and a product table 1.2.

Table 1.1: Character table of the C_{2v} pointgroup

$A_1, A_2, B_1, B_2 \dots$ symmetries

$E \dots$ identity

$\text{C}_2(z) \dots$ rotation about 180° around z-axis

$\sigma_v(xz / yz) \dots$ reflection at plane in xz or yz

	E	$\text{C}_2(z)$	$\sigma_v(xz)$	$\sigma_v(yz)$
A_1	1	1	1	1
A_2	1	1	-1	-1
B_1	1	-1	1	-1
B_2	1	-1	-1	1

The character table shows how symmetries change after applying different operations. A_1 has the highest symmetry meaning it does not change after using any of the operations shown in table 1.1. A_2 changes after reflection in xz- and yz-plane. B_1 changes after rotation of 180° around z-axis or reflection in yz-plane. And, finally, B_2 changes after

rotation around z-axis or reflection in the xz-plane. Additionally, a product table shows the combination of different symmetries. In group theory a combination of two elements of a group creates an element of the same group again.

Table 1.2: Product table of the C_{2V} pointgroup
 $A_1, A_2, B_1, B_2 \dots$ symmetries

	A_1	A_2	B_1	B_2
A_1	A_1	A_2	B_1	B_2
A_2	A_2	A_1	B_2	B_1
B_1	B_1	B_2	A_1	A_2
B_2	B_2	B_1	A_2	A_1

When talking about states in a molecule we notate the electronic states with capital letters ($A_1, A_2 \dots$), whereas vibrational levels are going to be written in small letters ($a_1, a_2 \dots$). The outcoming symmetry is indicated with upper case letters, which seems to be confusing in the first moment. One can understand it better by using a more classical picture: exciting different vibrational levels in a molecule will lead to different vibrations, where the whole symmetry can change. For example the symmetry is different if two CH_3 groups in acetone vibrate in phase or out of phase.

1.3 Acetone Literature

The fact that acetone has been studied for more than 40 years is a good indicator for how fascinating this simple ketone is. Scientists are still interested in acetone, especially in the time depended spectroscopy investigating its internal population transfer mechanism.

When talking about states in molecules some often repeated shortcuts are used to indicate the different states, transitions and orbitals [4]:

- non-bonding orbitals n
- bonding orbital, e.g., π - or σ -type
- anti bonding orbital, e.g., π^*

As example transitions from a non-bonding valence molecular orbital to higher states are written as ' $n-3s$ ' or ' $n-3p_x$ ' where $3p_x$ is the Rydberg orbital.

The interest was always also high in Rydberg states [5] due to their own special character being molecular orbitals but acting like atomic orbitals.

In acetone the excitation to high-lying Rydberg states is still popular for of theoretical

calculations and experiments. A very nice and detailed summary on the theoretical side was done by Diau et al. [6] and Shastri et al. [4] where one can see how different molecular orbitals look like and furthermore, they describe transitions from the ground state to 3s and 3p Rydberg states and the transitions to valence states π^* . Over the years a lot of femtochemistry groups were especially studying the 3p Rydberg states of acetone because they raise interesting questions. The 3p Rydberg states contain three electronic states called $3p_x$, $3p_y$ and $3p_z$, all having a different symmetry (A_2 , A_1 , B_2 , respectively) and furthermore, the high amount of vibrational levels allow new symmetry combinations as well [7]. Besides the symmetry aspects there are also different transition rules to these states. Here the transition to the $3p_x$ state plays an important role: While being dipole forbidden for one-photon excitation [8], the whole situation changes when multi-photon excitation is performed, resulting that $3p_x$ is not dipole forbidden anymore.

An experiment for excitation to the 3p states of acetone using resonant-enhanced multi-photon ionization (REMPI) was performed by McDiarmid and Sablijiic [9], where they studied the influence to transitions by using different polarized light to excite the 3p states and moreover, REMPI also allowed them to excite the $3p_x$ state (multi-photon process). This experiment also shows the influence of the gas pressure (here: 7 torr) resulting in broadened lines due to impact broadening. Furthermore, the vibrational levels demonstrate the different vibrational modes in a molecule [7] [6]. For a better interpretation of the spectra it is necessary to know which vibrational modes are excited [4].

In our group isolated acetone molecules in gas phase were studied using multiphoton processes and PEPICO. In the work of Paul Maierhofer et al. [10] in 2016, acetone molecules were excited by two photons (269 nm). After ionization the molecule can dissociate into an acetone parent ($C_3H_6O^+$) and an acetyl fragment ($C_2H_3O^+$). The temporal behaviour for different ionization channels was detected and moreover, it was determined if dissociation takes place in the neutral molecule or in the parent ion. As one example PEPICO allowed to observe that Norrish Type 1 (NT1) dissociation happens in the neutral molecule.

The previous work was followed by the detailed characterization of the fragmentation process from 5s to 8s Rydberg states by changing photon energy, pulse duration and pulse energy [11]. The activation energy, which leads to fragmentation of acetone to acetyl and methyl was determined with (0.79 ± 0.04) eV. Longer laser pulses (100-200 fs) increased the relaxation probability and as well, the fragmentation rate.

Another important study on acetone was the observation of the population transfer from high lying Rydberg states to lower one [12]. Three pump photons (400 nm) excite the molecule followed by the ionization with one probe photon (400 nm). The decay time constants were different for the states directly filled by photoexcitation (~ 320 fs) or indirectly filled by IC (~ 100 fs). The time constants were compared with previous works [10], [13], [14], [15], [16], [17]. Because PEPICO can only be performed at low counting rates,

Bayesian statistics [18] was be applied to analyse the data [24].

The results of the last paper [12] was the starting point of the current master's thesis. As written above it was observed that the low lying 3p Rydberg states can be filled from higher Rydberg states by internal conversion. The new goal was the direct excitation of the 3p states and verification if the time constants depend on the molecular symmetry of the state. Additionally, the theory group of Prof. Leticia Gonz  les calculated time constants using 'SHARC' [19] and expected that the decay time of the population depends on the different symmetries of the 3p states [8], [14]. The following work presents the preparation of the setup and as well, the first results, which already show the expected trend from theory.

The values for the energy levels in our experiment were taken by synchrotron measurements [8] where they used a wide excitation range from 3.7 eV up to 9.8 eV. However even when acetone was studied a lot using REMPI and recently also femotesecond experiments [14] were performed, there was never a real time tracking of the population behaviour of the 3p Rydberg states including vibrational coupling.

CHAPTER 2

Experimental

2.1 Overview

This section is going to present the enhancement of an existing pump-probe setup which was currently used to study relaxation dynamics of acetone in gas phase. Additionally, the optical setup is now combined with a new technique in our laboratory, being able to create helium nanodroplets (He_N).

The experimental part of this master's thesis strongly focuses on the optimization of the setup and the detailed description of the gas phase experiment. However, during this year the whole He_N -droplet setup was also constructed and is completely described in the master's thesis of Sascha Ranftl [20]. It should be mentioned that we are now able to switch between the acetone gas phase experiment and He_N -droplets relatively fast.

The starting point of this work with the existing setup can be found in the master's thesis of Paul Maierhofer [21], Markus Bainschab [22], Bernhard Thaler [23] and Pascal Heim [24].

To begin with the experimental part the most advance in the new setup was the implementation of important components which are used in both experiments at the moment:

- An **Optical Parametric Amplifier** (OPA) to have a wide range of wavelengths: 240-2600 nm,
- a **Prism Compressor** to increase the temporal resolution by compensating the

positive chirp from the OPA ,

- a lot of new **optics** which are be described in detail in the following section

The basic principle of the pump-probe experiment is shown in figure 2.1: The generated beam from the Legend Laser System (800 nm central wavelength, 25 fs pulse duration, 13 W output power, 25 kHz repetition rate) is split right after the output with a beam splitter into a pump path and a probe path. After passing a lot of optics (e.g. mirrors, crystals) both beams are focused into the measurement chamber, where the molecules are excited by the pump pulse, the probe pulse ionizes it and finally, electrons and ions are observed. By applying a negative (for e^-) or positive (for i^+) voltage on a repeller the particles are pushed into a time of flight tube. In the current setup we are still able to perform PEPICO (Photoelectron Photoion Coincidence) spectroscopy using an ultrafast switch [22], however, the following experiment only focuses on the detection of the electrons which is done using their kinetic energies as observable. When electrons or ions hit a micro channel plate (MCP) they are detected and the analysis of the created data is done with different software and programs, mainly written in MatLab. Furthermore, with a quadrupol mass spectrometer (QMS [20]) we are able to check which sort of atoms appears in the measurement chamber.

To continue, the setup will be described in detail: It starts with the whole optical setup, followed by the new components, namely OPA and prism compressor.

At the end of this section the pressure readout which is done using a Raspberry Pi in combination with Python scripts, is described.

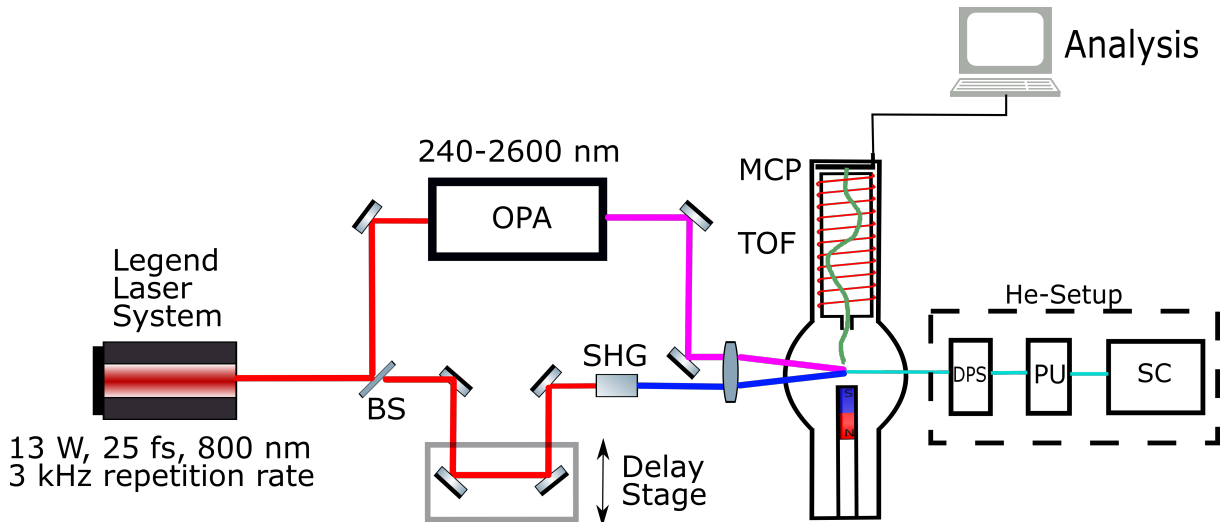


Figure 2.1: The basic setup for the gas phase experiment and He_N-droplets. This setup includes the Legend Laser System, pump and probe path, time of flight spectrometer and analysis tools.

2.1.1 Optical Setup

The first section starts with the complex optical setup, presented in figure 2.2.

The horizontal polarized laser beam is split with a beam splitter (BS1, 80 % reflectivity). The high intense reflected part is lead into the OPA and indicates the pump path in this experiment. M1 couples the beam into the OPA where the fundamental 800 nm wavelength is frequency converted to set the desired wavelengths. After the OPA, the beam passes a prism compressor to reduce the temporal duration of the pulse. The working principle of the OPA and the prism compressor is described later (see chapters 2.2 and 2.4). With the wire grid polarizer the power of the OPA path is regulated. Mirror M2 leads the beam on a lens ($f=1000$ mm) and finally, it enters the measurement chamber.

For the probe path the transmitted part of BS1 is used and additionally, split again with BS2 (30 % reflectivity) where the low intense reflected part enters the transient absorption setup, which is build by Leonhard Treiber [25].

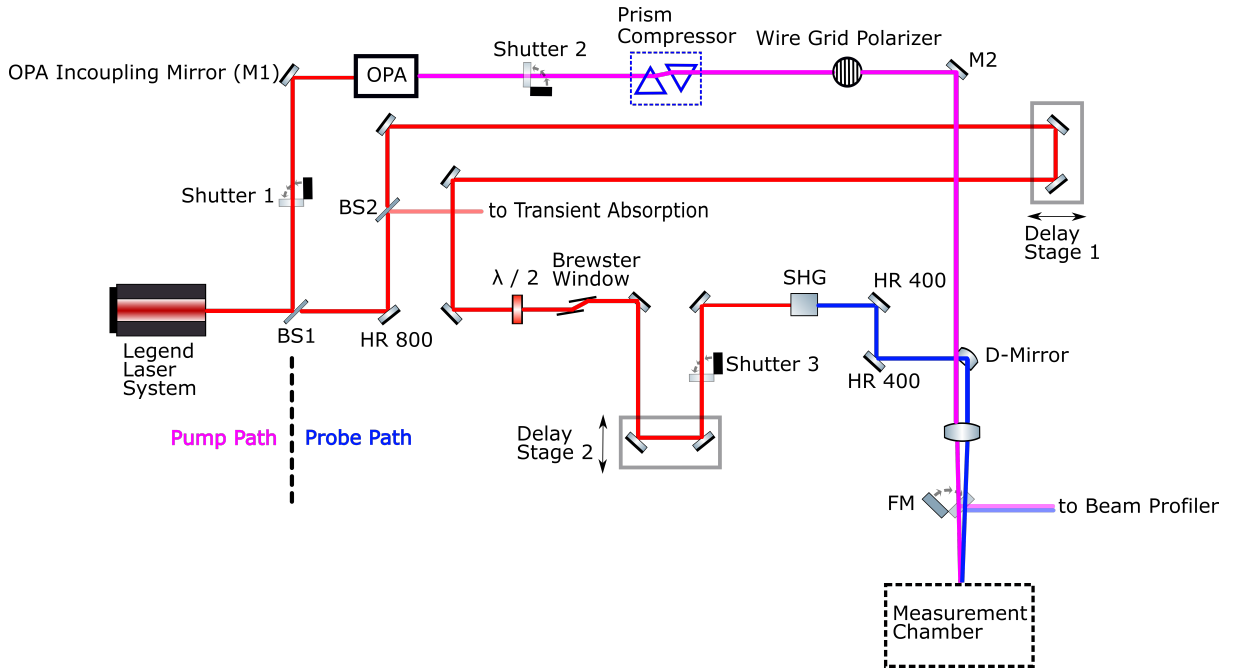


Figure 2.2: The whole optical setup with all important components: OPA, prism compressor, wire grid polarizer, delay stages and beam profiler.

The remaining transmitted part from beam splitter BS1 passes a first stage, called delay stage 1. This stage is used to adjust the path length of the probe path. Inside of the OPA the beam path increases the path length by 3.6 m, so it is necessary to compensate this by extending the probe path. The total path length is about 126.5 cm.

After passing delay stage 1 a $\lambda/2$ - plate and a brewster window control the output power

of the probe path, simply by changing the polarization direction of the light. Afterwards, stage 2 delays the probe pulse in time to do pump-probe experiments. This stage is actuated with a motor and able to move in μm steps.

BBO or LBO crystals create non linear optical processes (here: second harmonic generation, SHG). A D-mirror (90 % reflectivity for 250-450 nm) leads the beam on the lens and then this beam enters the measurement chamber.

With a flipping mirror (FM) both beams are directed at a beam profiler to find the spatial overlap. The beam profiler includes a camera with a CCD chip. The intensity of the beam is lowered with an ODE filter to make sure the CCD chip is not destroyed. The camera is read out in Matlab with 'Copy_of_profile_horver.m', where both beams become visible on the screen to find and adjust the spatial overlap for the pump and probe beam. This is very important because in a pump-probe experiment the two pulses have to overlap in space and time.

The next improvement was the implementation of the three shutters, namely Shutter 1, Shutter 2 and Shutter 3. All shutters are controlled with an Arduino and are called in MatLab with 'PPShutter.m' [23]. These shutters are used in the following cases:

- Shutter 1 blocks the whole OPA beam. This shutter is used in combination with an OPA safety box (see chapter 2.2.4) . Shutter 1 closes when the OPA output power undergoes a trigger level. This could happen, for example if the output beam of the Legend has a beam walk during night due to thermal effects. Then the whole beam path inside the OPA changes too and in the worst case optics are damaged.
- Shutter 2 and Shutter 3 can block the pump path and probe path separately, e.g. to do pump / probe - only measurements.

All shutters work fully atomized. This nice feature allows to perform long time measurements and additionally, pump- and probe- only spectra can be taken to check if the overlap got lost or if the output power is not stable.

2.1.2 Parameters of SHG Crystals

In our experiment we perform pump-probe spectroscopy to high lying Rydberg states in acetone [1], [15], [14], [4]. These parallel states are filled by the pump pulse (here: 333 nm) and afterwards a probe pulse (401 nm) empties the state. As consequence the energy resolution strongly depends on the chosen probe crystal. In our laboratory we have five crystals with different sizes at the moment: 100 μm , 200 μm , 500 μm , 1000 μm , 5000 μm . It was important to use the right crystal to guarantee that all three Rydberg states are visible separately (shown in figure 4.1). In general the energy is given by $E = h \cdot \nu = \frac{h \cdot c}{\lambda}$ with $c = \lambda \cdot \nu$, where E is the energy, h the Planck constant, ν the frequency, c the speed of light and λ the wavelength. The wavelength is indirect proportional to the energy, so it is not possible to calculate the energy resolution from the full width half maximum (FWHM) directly .

In table 2.1 all SHG crystals in our laboratory are listed. The spectrum of every crystal was measured with an Ocean Optics spectrometer. The number of the spectrum file and measurement date are shown in the comment column. From every spectrum the FWHM was fitted using a Gaussian fit model and furthermore, with this information the energy resolution was calculated.

Additionally, in table 2.1 the transform limit of each crystal is noted. This is necessary because the time-bandwidth product $\Delta E \cdot \Delta \tau = \text{const.}$ has the consequence that a good energy resolution has a bad temporal resolution and vice versa. The phase-matching bandwidth [26] decreases with thicker crystals of length l . This is the reason why, for example, the 5000 μm crystal has a sharper energy spectrum (good energy resolution) then the 100 μm crystal, while having a poor temporal resolution. The chosen SHG crystal in this experiment (1000 μm , see table 2.1) was a compromise between a good energy resolution and a sufficient temporal resolution.

Finally, the complete energy resolution $\Delta E_{\text{res}, 1}$ in table 2.1 of the setup, combining resolutions of TOF and SHG crystals, was calculated in the following way and using these quantities:

$E_{\text{TOF}} \cdots$ energy resolution of the TOF spectrometer

$E_{\text{SHG}} \cdots$ energy resolution of the SHG crystal

$\Delta E_{\text{res}, 1} \cdots$ energy resolution of the setup for different SHG crystals with length l

$$\text{with } \Delta E_{\text{res}, 1} = \sqrt{E_{\text{SHG}}^2 + E_{\text{TOF}}^2}$$

1. With the 1000 μm SHG crystal a photoelectron (PE) spectrum was taken, shown in figure 2.3. This spectrum includes the complete information of the energy resolution for both beam paths

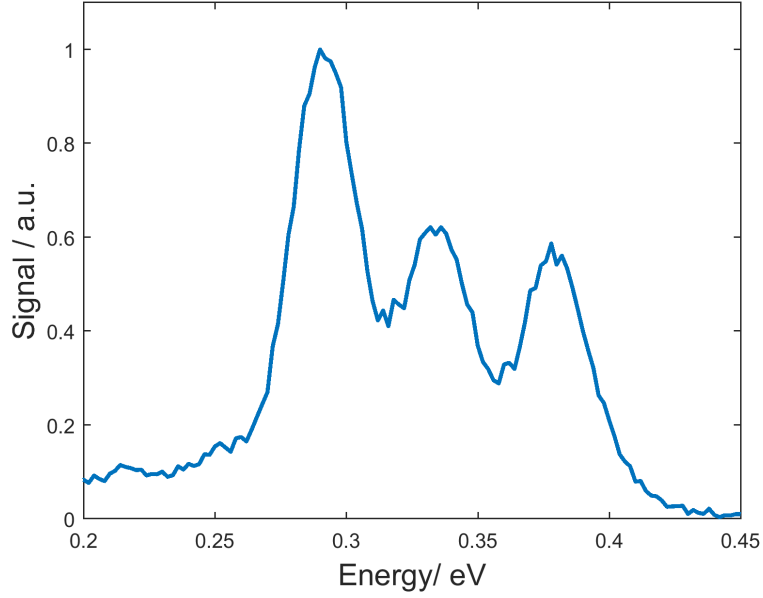


Figure 2.3: PE spectrum using a 1000 μm crystal in the probe path.
Measurement date: 19.10.2017, eiTOF number: 4849

2. From this spectrum the energy resolution using the low determined peak was calculated: $\Delta E_{\text{res}, 1000 \mu\text{m}} = 0.31 - 0.276 = 0.034 \text{ eV}$
3. The energy resolution of the TOF can be calculated with $E_{\text{TOF}} = \sqrt{\Delta E_{\text{res}, 1000 \mu\text{m}}^2 - E_{\text{SHG}}^2}$ and does not change for constant repeller voltages:
 $E_{\text{TOF}} = \sqrt{0.034^2 - 0.026^2} = 0.022 \text{ eV}$
4. The energy resolution $\Delta E_{\text{res}, 1}$ for different crystals is calculated
 $\Delta E_{\text{res}, 1} = \sqrt{E_{\text{TOF}}^2 + E_{\text{SHG}}^2}$ and is listed for every SHG crystal in table 2.1

Table 2.1: List of the SHG crystals in the laboratory

$l \cdots$ length of the crystal

$\sigma_{\text{FWHM}} \cdots$ spectral width (full width half maximum) of the crystal

$E_{\text{SHG}} \cdots$ energy resolution of the SHG crystal

$\tau_{\text{TL}} \cdots$ transformlimit

$\Delta E_{\text{res}, 1} \cdots$ energy resolution of the setup for different SHG crystals of length l

$l / \mu\text{m}$	$\sigma_{\text{FWHM}} / \text{nm}$	$E_{\text{SHG}} / \text{eV}$	$\tau_{\text{TL}} / \text{fs}$	$\Delta E_{\text{res}, 1} / \text{eV}$	Comment
100	8.4	0.065	29	0.072	Nr. 334; 28.08.2017
200	6.6	0.050	37	0.054	Nr. 335; 28.08.2017
500	4.2	0.032	56	0.039	Nr. 338; 30.08.2017
1000	3.4	0.026	71	0.034	Nr. 374; 02.10.2017
5000	1.9	0.015	195	0.027	Nr. 428; 12.12.2017

The energy resolution was calculated with the FWHM of the left peak in figure 2.3 using the Matlab cursor. This method has the problem that the underground from 0.2 eV to 0.25 eV can sophisticate the values. A better solution is to use a Gaussian fit model and take the FWHM from the fit parameter, as demonstrated in the electron spectrum in figure 2.4. This figure shows the percentage of the three single Gaussian fits for each peak. The combination of these three fits gives the triple Gaussian fit, like shown in figure 4.2. The fits start at energies > 0.25 eV to avoid the background. For the fit model

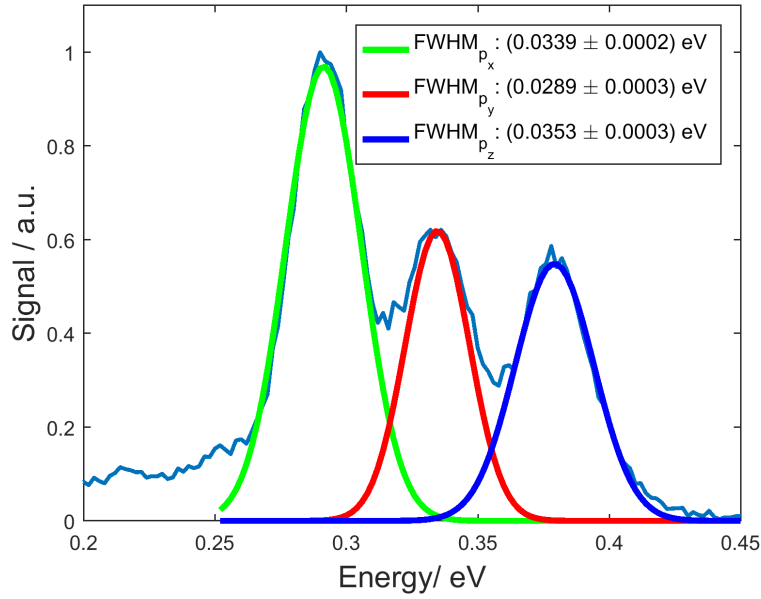


Figure 2.4: Three single Gaussian fits and FWHM of each fit. Green: $3p_x$, red: $3p_y$, blue: $3p_z$.

the amplitude, the position of each peak and the standard deviation was set free. The FWHM of the three peaks are fitted and have the following values: (0.0339 ± 0.0002) eV, (0.0289 ± 0.0003) eV and (0.0353 ± 0.0003) eV for $3p_x$, $3p_y$ and $3p_z$, respectively. For the calculation of the energy resolution the most dominant peak (here: left peak, $3p_x$) was chosen. The FWHM of the $3p_x$ peak is still in a good agreement with the calculation which was done above (0.0034 eV). For the $3p_y$ peak the fit does not match well, as seen in figure 2.4, because the value is too low compared to $3p_x$ and $3p_z$. This can be explained because the $3p_y$ peak overlaps with parts of $3p_x$ and $3p_z$.

The best energy resolution of our TOF was estimated with $\frac{\Delta E}{E} = 4\%$ [27].

Using the fitted values of $3p_x$ in figure 2.4 the energy resolution of the TOF in is given by $\frac{\Delta E}{E} = \frac{0.0339}{0.292} = 12\%$.

2.1.3 TOF Energy Resolution

Here is a short summary of the working principle of our time of flight (TOF) spectrometer shown in figure 2.5.

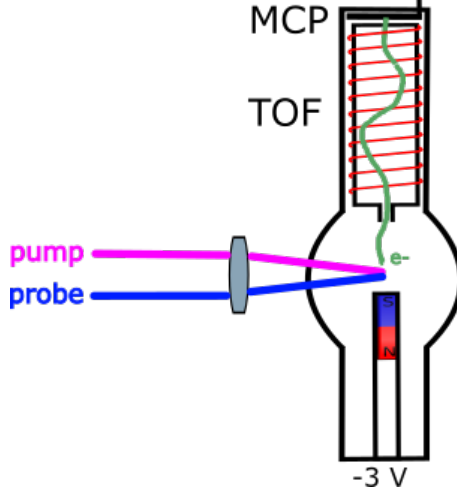


Figure 2.5: Basic principle of our time of flight spectrometer: pump and probe pulses are focused into the measurement chamber where e^- or i^+ are pushed into the flight tube using different repeller voltages.

A lens focuses the pump and probe beam into the with acetone gas filled measurement chamber, where the pump-probe process creates electrons and ions. The observable for electrons is their kinetic energy (E_{kin}) and for ions it's their mass to charge ratio ($\frac{m}{q}$).

Using a repeller with a negative or positive voltage, electrons or ions are pushed into the time of flight tube. In our setup we combine a TOF spectrometer with a magnetic bottle to increase the collection efficiency. The charged particles move along a circular path due to the Lorentz force. The inhomogeneous magnetic field is much stronger at the ionization region (repeller) then in the flight tube, where the constant magnetic flux redirects the velocities of the electrons [22]. In a magnetic bottle spectrometer the particles do not pick up energy from the magnetic field.

Afterwards, they hit a MCP detector and can be analysed. For the detailed description how every component works exactly and how the evaluation of the flight times takes place please read the master's thesis of Markus Bainschab [22] and Bernhard Thaler [23].

The description of the experiment continues with the influence of a very critical parameter: The energy resolution. This quantity is so important due to the fact that the 3p Rydberg states are very close together and so it is necessary to have a good energy resolution to see them separated in the PE spectrum.

The energy resolution of the whole setup is limited by two factors: The TOF spectrometer

and the used crystals in the probe path.

In case of the crystals the 1000 μm BBO crystal was chosen (see table 2.1), because this crystal has the needed energy resolution to resolve the three peaks of the 3p states in the electron spectra, while having a better temporal resolution than the 5000 μm LBO crystal.

The energy resolution of our TOF estimated by [27]

$$\frac{\Delta E}{E} = 4\% \tag{2.1}$$

where E is the kinetic energy of the electrons. For the current setup $\frac{\Delta E}{E} = 12\%$ was calculated in chapter 2.1.2 . The energy resolution becomes a lot better by changing the repeller voltage to more positive values. This leads to a reduction of the kinetic energy of the electrons, so they have a longer flight time to travel through the tube. Because of the relation in formula (2.1) a smaller E also decreases ΔE . With this conclusion the energy resolution became greatly better. Additionally, the energy resolution can be improved by moving the repeller down in z-direction to affect the trajectories of electrons.

A characterisation measurement of electron spectra for different repeller voltages is presented in chapter 3.1.

2.2 Optical Parametric Amplifier (OPA)

During this master's thesis the implementation of the OPA in the setup was a huge step forward. Now we are able to set our wavelengths in a wide range of 240-2600 nm. The stabilization of the OPA output power (pulse to pulse fluctuations $< 2\%$) allows us to use it for gas phase experiments and He_N -droplets. During this year we also found a daily routine for coupling in the 800 nm pump laser, which gives us a better understanding of the whole OPA process inside and furthermore, we are able to adjust it in a save way.

2.2.1 Basics

An optical parametric amplifier works the following way: two beams called signal ω_s and idler ω_i are created from one incoming pump beam ω_p where the frequencies satisfy the following condition: $\omega_p = \omega_s + \omega_i$. Energy and momentum are conserved for signal and idler beam. In the amplifying process one of the output beams is amplified by overlapping it with the pump beam.

The OPA in our laboratory is more complex and works in two amplifying stages. Figure 2.6 shows the whole beam path of our OPA. How the whole beam path looks like can be found in the OPA manual [28]. Figure 2.7 cuts down the complex process in a simple block diagram and presents as example the creation of 333 nm output wavelength: The 800 nm pump beam is split with a beam splitter (80-98% reflectivity, depending on the input pump energy) into two parts (1). One part is used for white light generation (2) (χ -3 effect). The white light has a stretched spectrum, containing lots of frequencies. To set a wavelength, the remaining red part of the pump pulse is overlapped with a chosen wavelength range $\Delta\lambda$ of the white light spectrum (3). This is done in the pre-amplifier (green box). In the second amplification step the created beam (4) is overlapped again with the pump beam (5) and amplified (yellow box). The wavelength of the beam who leaves the OPA is created by different non linear processes (here: SHG, blue box) or mixing. A detailed description of every wavelength region is shown in the appendix C.

2.2.2 Working Principle and Power Optimization of our OPA

Here all important components of the OPA as well as the in-coupling routine are described in detail.

Figure 2.8 shows how the OPA in this lab looks like with opened cover. The red line indicates the high power 800 nm part (~ 11 W) from BS1 in figure 2.2 and shows where the beam enters the OPA till it hits the closed shutter. It is very critical if this beam path changes but for case it happens, the readjustment has to be done with BS1 and M1.

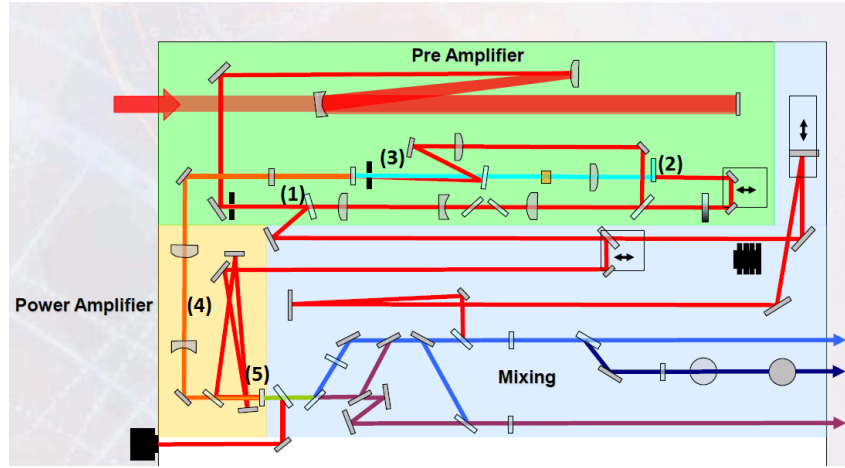


Figure 2.6: Beam path through the OPA, chosen from the manual [28].

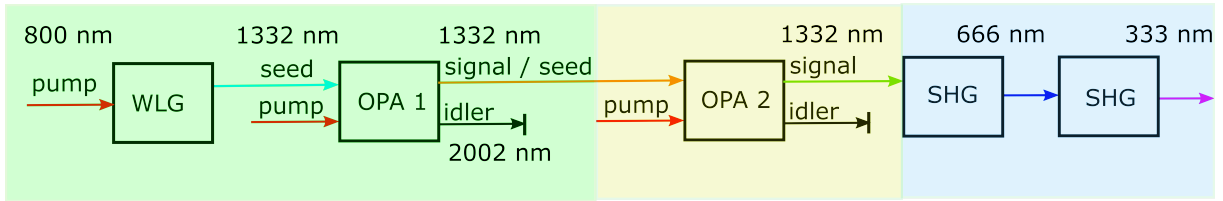


Figure 2.7: Reduction of the complex system in figure 2.6 to an easier understandable block diagram to demonstrate how 333 nm is created.

The blue circles contain the OPA shutter, which is controlled by the software 'WinTopics', and the spot where a safety aperture is build in. The OPA shutter and alignment aperture are always used at the beginning of the in-coupling process to check if the incoming beam goes correctly through all optics. This is checked by eye if the red-light pump beam goes through the alignment aperture.

Finally, the green circles demonstrate the four components which are used to select the wavelength range and to maximize the output power.

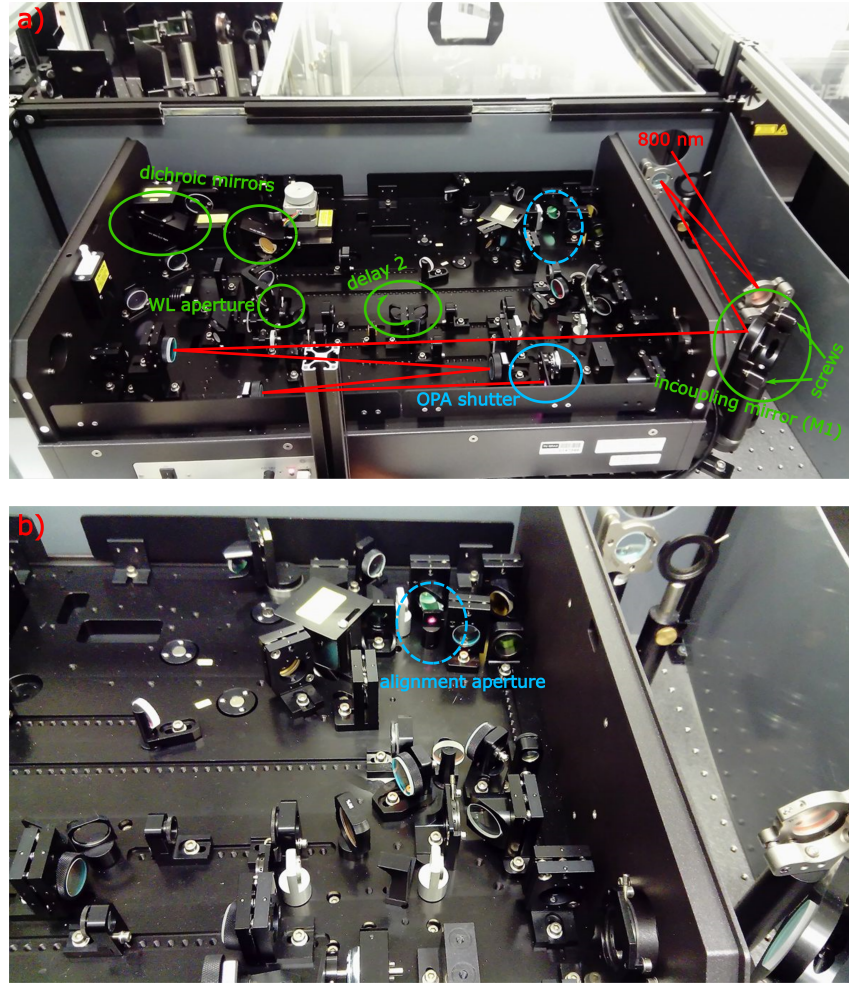


Figure 2.8: Adjustment of the OPA: Figure a) shows all its important components. Red line: incoming beam from the Legend laser. Blue circles: Spots which should be checked in the first in-coupling routine. Green circles: The four components which are used when maximizing output power and stability. Figure b) shows where a alignment aperture is placed to check if the beam goes through the OPA correctly.

Dichroic Mirror List

Table 2.2 lists all dichroic mirrors from figure 2.8 and their transmission range. In this experiment (pump wavelength $\lambda = 333 \text{ nm}$) the first mirror is the one with a range of 720-970 nm and the second mirror has 275-350 nm transmission range.

Table 2.2: Dichroic mirrors which can be build in the OPA to set the wavelength range $\lambda \dots$ wavelength

OPA dichroic mirrors
λ / nm
955 - 1150
720 - 970
530 - 730
410 - 540
275 - 350
230 - 290

Daily OPA In-coupling Routine

Every time after the Legend Laser is turned on it takes about three hours until the system is thermally stable. During this time the OPA is blocked out but afterwards the following rough incoupling process checks if the beam passes the OPA correctly and if some output power is observed:

- Decrease the round trips of the Legend laser from 4246.25 ns to 4216.25 ns (stand: January 2018) with delay 2.
- Open OPA cover.
- Check position of incoming pump beam on OPA shutter (blue circles in figure 2.8).
- Insert a alignment aperture and look if the beam goes through (blue circles in figure 2.8).
- If the last two points are o.k. take the aperture out and turn the round trips to 4246.25 ns again. If not use M1 and/or BS1 to adjust the beam path.
- Be careful to use the right dichroic mirrors (see table 2.2). Otherwise there is no or very low output power.
- Check again at opened cover if no damage of the optics is observed.
- If everything works correctly, one should be able to measure the output power with the pulse meter.
- Close OPA cover.

The OPA itself needs about 12 hours to be thermally stable but then the output power can be maximized as described in the following:

Optimizing the Output Power

The next steps show how the output power is optimized to its maximum. In general the OPA has four components, all indicate as green circle in figure 2.8, which are adjusted in the daily in-coupling routine.

Side note: If 'WinTopics' crashes all motors have to be reset which is done in WinTopics → Motors → Direct Access → reset. If the software crashes the wavelength range in the program has to be set new.

- **The in-coupling mirror (M1):** The vertical and horizontal position of the beam is set with two screws. Be extremely careful when changing the horizontal direction of the beam. In this direction the change of the beam is very sensitive resulting that a small change can lead the beam different through the OPA.
- **The white light:** is adjusted with an aperture and is different for every chirp position. If the aperture is on its opening limit and the white light still looks bad, a compensator plate can be used to improve the white light. The compensator plate is simply a round plate with different thicknesses. An example of good and bad white light is shown in the OPA manual [28].
- **The chirp:** is adjusted with the grating compressor at the output of the Legend laser. Pressing '+' or '-' on the control panel changes the distance between the gratings. In this way the chirp and furthermore, the output power can be adjusted to its maximum value. Unfortunately the grating compressor changes the chirp of probe path too, so always check the SHG output power after changing the chirp with the control panel.
- **Delay 2** (Attention: This is not delay 2 which is used to reduce the round trips. It is set in software WinTopics → Motors → Direct Access): By changing this value the output power can be increased. Delay 2 is a rotation stage and can not move in x- or y-direction. This stage rotates two glass plates, shown in figure 2.8, putting more or less glass into the path to optimize the optical delay between pump and seed beam.

Furthermore, these four components also depend on each other, this is the reason why the maximization of the output power is an iterative process: After the OPA system is thermally stable as mentioned above the first step is to increase the output power with M1 to its current maximum possible value. For the case the OPA was blocked out for

some time it takes again some hours till it reaches thermal equilibrium again.

Then the in-coupling process continues by adjusting the white light. Use a white card to see if the white light looks okay. Always block out the incoming beam before putting the white card into the beam to minimize the risk of damaging optics. Be very careful because the incoming beam enters the OPA with about 11 W.

Continue with changing the chirp with respect to the output power. It should be mentioned that this changes the white light too but there is always a best configuration for the white light depending on each chirp position.

Finally, use delay 2 to increase the output power.

If there are low output powers and / or bad stabilities after an iteration step try to change the white light again followed by chirp and delay 2. It is not possible to get higher output powers with by changing M1 if the system is already thermally stable. Just readjust M1 again if the 800 nm pump beam was blocked out for some time.

The fine tuning of the stability is only done with chirp and / or delay 2. It should be mentioned that sometimes it can be enough just to change on of these last two parameters. It was observed that the chirp had the most influence to the stability, when the output power was maximized with delay 2 before.

To summarize, the in-coupling process for the rough tuning is done with all four components, including mirror M1, followed by white light check, chirp and delay 2. For the fine tuning chirp and delay 2 are used.

2.2.3 Stability of the OPA

To perform successful measurements it is necessary to have a good stability of the OPA output power. This means that the pulse to pulse fluctuations should be lower than 2%. Basically the stability of the OPA is given by two important factors:

- The in-coupling process and
- thermal fluctuations.

The in-coupling process is described in section 2.2.2. A well adjusted OPA works near its maximum output power level for each wavelength range. The absolute value of the output power strongly depends on the chosen wavelengths. Furthermore, the OPA runs less stable the closer it comes to the wavelength range limits.

Thermal fluctuations, induced for example by the air cooling system or an open OPA cover, leads to mechanic strains of the optics inside of the OPA. To minimize these thermal effects we linked the OPA to our water cooling system and additionally, we surrounded the whole experimental setup with plexiglass plates. The adjustment of the output power

should be performed with closed OPA cover. Otherwise, higher absolute output powers are observed, but they result from strong fluctuations and are unwanted artefacts.

2.2.4 OPA Security Box

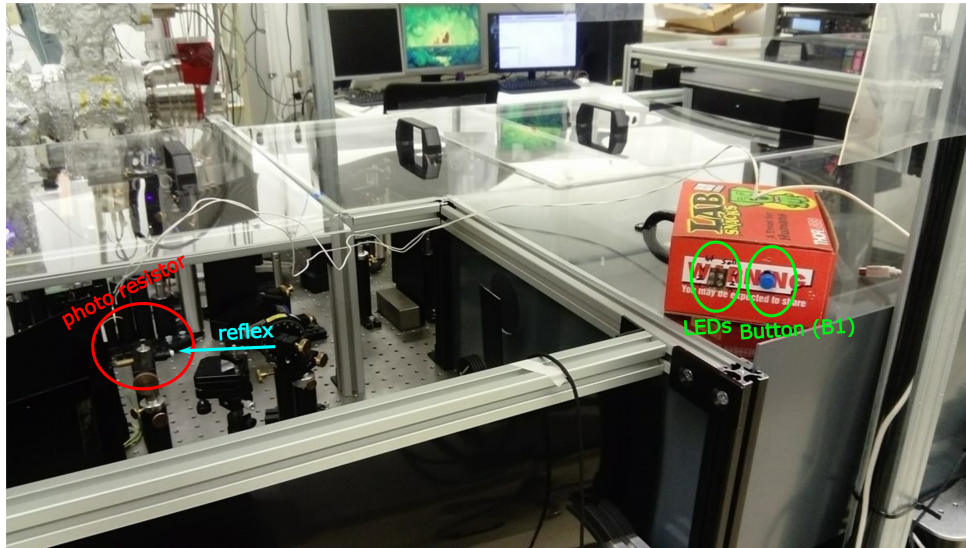


Figure 2.9: The OPA security box where a photo resistor is used to measure a reflex (blue arrow) from the WGP. The electronics of the box is build in the red box. LEDs indicate the trigger level and intensity of the reflex. Button 1 is used to open shutter 1 by hand.

Figure 2.9 shows the security box which was build by Pascal Heim and implemented to monitor the OPA during night and moreover, to be able to perform measurements during this time.

The security box consists of a photo resistor as sensor and an electrical board inside the red box. An USB B cable is plugged in to connect the red box with the power supply. The whole control takes places with an Arduino.

The photo resistor is build in between prism compressor and wire grid polarizer (WGP), using a reflex from the WGP (blue arrow) with enough power. The intensity is indicated by three LEDs (white LEDs) on the OPA box and additionally, a trigger level can be set manually with a potentiometer (green LEDs). If there is a drastic beam walk during the measurement the reflected beam will not hit the photo resistor anymore and shutter 1 (figure 2.2) closes immediately. This is a save way to make sure no optics inside of the OPA are damaged. Pressing and holding B1 allows to open shutter 1 manually.

2.3 How to Find and Shift Temporal Overlap

When doing acetone measurements the temporal overlap is hard to find due to the fast (femtoseconds) relaxations dynamics. This problem can be avoided with indium: The first excited state of indium has a lifetime of some nanoseconds. It is easier to find the temporal overlap with indium first, as demonstrated in figure 2.10, and switch back to acetone then.

The shift of the temporal overlap is done with stage 1. Changing stage 1 decides where the temporal overlap appears on stage 2. The following figure shows an example how an indium time scan looks like: Figure 2.10 shows the time delay between pump and probe pulse (left: in ps, right: in mm). Light travels 0.3 mm in 1 ps.

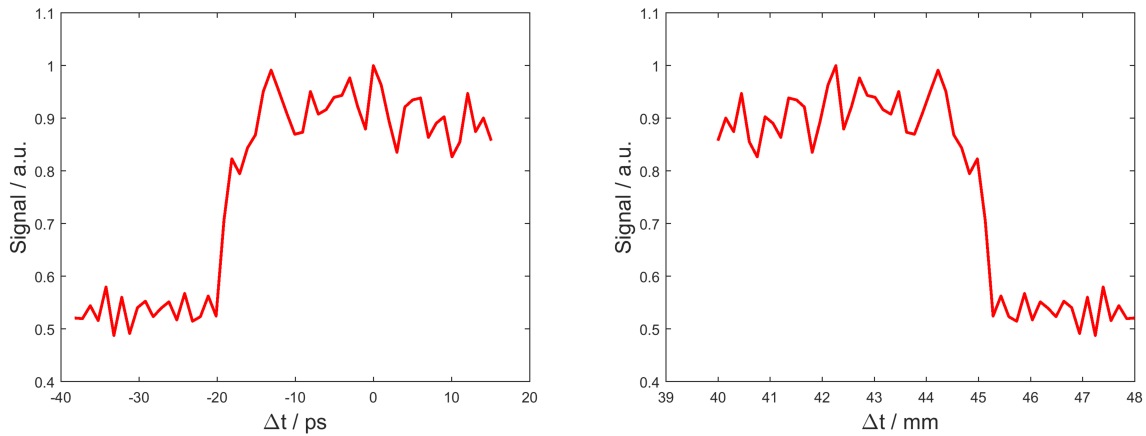


Figure 2.10: Typical electron time scan with indium. The left figure shows the temporal overlap in time in ps, the right figure indicates the position of the overlap on stage 2 in mm. Pump wavelength: 375 nm, probe wavelength: 420 nm. Measurement date: 28.07.2017

This time scan demonstrate perfectly how an overlap signal for a long living excited state should look like. If pump and probe pulse do not overlap temporally the resulting signal is just the sum of pump-only counts and probe-only counts (low signal side in both scans). As already mentioned the pump pulse populates the excited state and the probe pulse depletes it. Changing the time delay between pump and probe pulse scans the population of the excited state and shows their dynamics. The position of the overlap is observable in a sudden raise of the signal. Furthermore, the overlap position gives the time zero point where pump and probe pulse perfectly overlap in time. In our setup the position is indicated on delay stage 2.

We can shift the overlap position on delay stage 2 with delay stage 1. Stage 1 delays the probe path with respect to the pump path. The point of overlap indicates where both beam paths have the same length. Therefore, stage 1 shifts the position of the overlap on

stage 2 by increasing / decreasing the path length.

For example, if one is more interested in the dynamic side (high signal), it is necessary to shift the overlap to smaller time delays, where the probe pulse appears earlier. To change the overlap from 20 mm to 47 mm (low signal side) can be done by increasing the path length of stage 1 by 27 mm.

Or in other words: Increasing the path length of stage 1 shifts the temporal overlap on stage 2 to higher time delays (in ps) but lower position values (in mm) and vice versa.

Side note: At the moment position 50 mm on stage 2 is the starting point.

2.4 Prism Compressor

The beam in the OPA passes a lot of material, so the beam at the OPA output is positively chirped because of dispersion. This basically means that the red part of the light moves faster through the material than the blue part. To compensate this effect it is necessary to delay the red part of the light. This can be done with a prism compressor. A prism compressor arrangement of four prisms is shown in figure 2.11. Every prism is aligned in such a way that the incoming beam always enters every prism with Brewster's angle. The red part has a longer optical way then the blue part now by moving more or less glass into the beam path. A detailed description can be found the manual from 'Newport' [29]. In summary, a prism compressor is a setup that allows to add positive or negative chirp by putting more or less glass into the beam path.

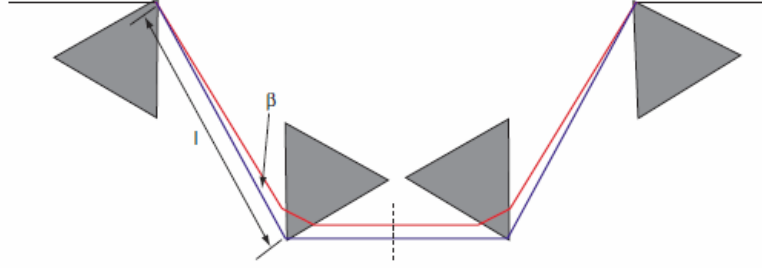


Figure 2.11: Working principle of a prism compressor: The prisms are arranged in a configuration that the red part of the light is delayed by having a longer optical path through the prisms compared to the blue part. The dashed line indicates the mirror point. The picture is taken from the Newport manual [29].

To minimize the size of a prism compressor setup and make it more compact one can build in a mirror after the second prism, which is called the mirror point (dashed line in figure 2.11). In our current setup we use a prism compressor with folded geometry as shown in figure 2.12. In a folded geometry construction a D-mirror is build in at the mirror point. The reflected beam goes under the incoming beam the same way back and is coupled out with a D-mirror.

2.4.1 Adjusting the Prism Compressor in General

When the wavelength of the OPA is changed, the beam path inside of the OPA is different. So the outcoming beam hits the first prism with different angle then before and as consequence the prism compressor has to be re-adjusted whenever the wavelength is changed.

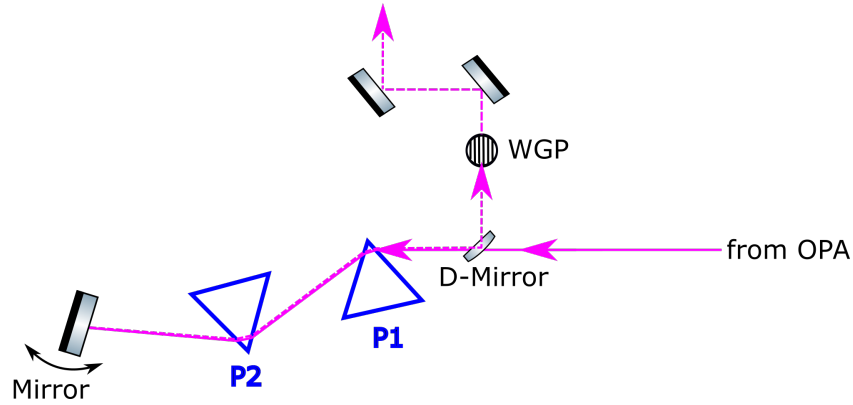


Figure 2.12: A folded geometry prism compressor as used in our laboratory.

Figure 2.13 presents how the prism compressor in our laboratory looks like including all its components and beam path through it.

Here is an basic instruction how to build up and adjust the prism compressor when it is build in for the first time. The improvement of the temporal resolution is shown in detail in chapter 3.

1. Adjust prism 2 in a way that the apex-apex distance between both prisms (point to point) is exactly 270 mm. This value depends on the chosen wavelength.
2. Adjust the position of prism 2 fine, so that the prism stage is in the middle position and that the incident beam is on the middle of the incident plane of the prism.
3. Adjust prism 2 angle so that the refracted beam angle is minimized (Brewster's angle incidence, checked with white card).
4. Adjust mirror behind prism 2 so that the incoming and outgoing beam have the same path (best with a white card holding between the prisms).
5. Adjust the position of the wire grid polarizer behind the D-mirror so that there is no reflex. Attention: Rotating the polarizer seems to change the angle of the reflected beam.

The difference between a good and a bad temporal resolution is described in chapter 3.2.

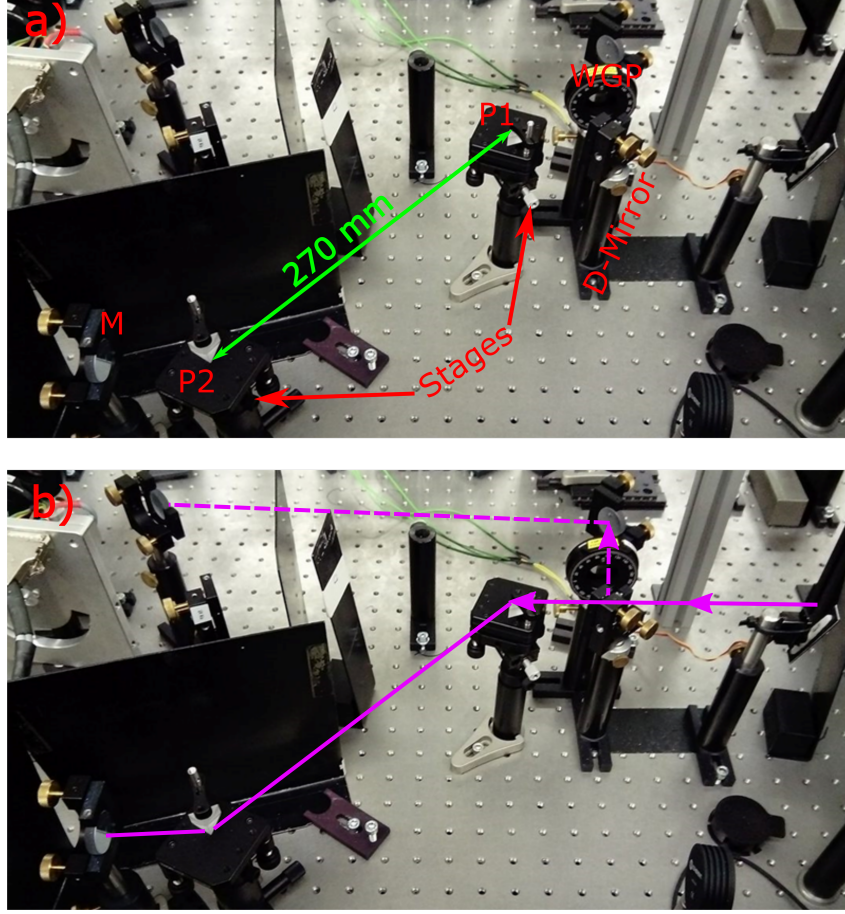


Figure 2.13: Prism compressor of our laboratory. Figure a) includes all its components. Figure b) shows the beam path. The dashed line is the reflected beam after the mirror and goes under the incoming beam. The power is set with a wire grid polarizer.

2.4.2 Improving the Temporal Resolution

The group delay dispersion (GDD) of the prism compressor is always negative and given by [29]:

$$GDD_{\text{prism}} = \frac{\lambda^3}{2\pi c^2} \left[-4l \left\{ 2 \left(\frac{dn}{d\lambda} \right)^2 \right\} + 4 \left(\frac{d^2n}{d\lambda^2} \right) (2D_{1/e^2}) \right] \quad (2.2)$$

where λ is the wavelength of the light, c is the speed of light, l is the distance between apex 1 and apex 2, n is the refractive index and D_{1/e^2} is the beam diameter at $1/e^2$. The first term which includes l is always negative, the second term always positive. Equation 2.2 is the short formula of the GDD. If someone wants to do a detailed calculation, use the original formula, which can be also found in the Newport manual [29] in equation (12).

The basic adjustment of the prism compressor is done in two steps: As shown in formula

2.2, the distance l between both prisms strongly depends on the chosen wavelength λ . When the wavelength is changed, l has to be readjusted to get the same GDD as before. The fine tuning can be done by moving both prism on their stage.

The separation of the prisms depends on the wavelength and is 270 mm in this setup at the moment. As mentioned before the GDD is always negative and putting more or less glass into the beam path changes the second term in formula 2.2. As result the GDD becomes more or less negative.

The temporal resolution can be improved by arranging both prisms in the following way: Move both prisms on their small stage and measure the cross correlation at three points:

- maximal distance with respect to the door
- minimal distance with respect to the door
- middle distance with respect to the door

Due to dispersion the arrangement is always different and has to be checked again for every change of the wavelength.

As shown in formula 2.2 the GDD depends on the distance between the prisms l . In the latest tests changing the distance between the prisms did not influence the cross correlation for the current wavelengths.

2.5 Raspberry Pi

We are able to read out the pressure values in our measurement chambers online at: <https://fexphrpifslab.tugraz.at/oversight/>.

Figure 2.14 shows the principle flowchart of the webserver process. A detailed description was written in the master's thesis of Florian Appoloner [30].

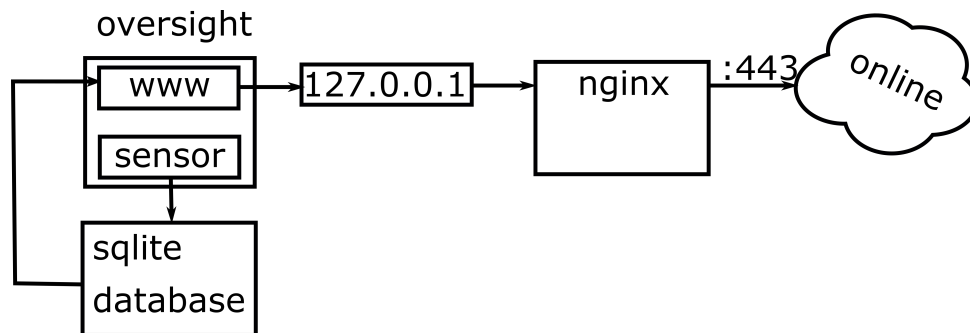


Figure 2.14: Flow chart how our homepage works in principle.

The pressure monitoring is done with an application called 'oversight'. Oversight contains two elements: homepage (www) and sensor. The homepage is created with django, a standard web framework written in Python. A detailed introduction how to build a new homepage with django can be found online [31].

A sqlite database stores the data of the sensors and they are updated every minute on the homepage. Furthermore, a nginx server is used to put the homepage online. All sensors are read out with Python scripts, namely pressure.py and MCP3008.py. The full codes of these programs including their description are listed in the appendix B.4 and B.2.

2.5.1 General Information about our Raspberry Pi

- Model: Pi 2 Model B v1.1
- Pin assignment: see appendix A or [32]
- Remote host: 129.27.156.183
- Username=pi; password=fslab1234; username and password for the homepage can be found in the OneNote: LabBook/Miscs/Raspberry Pi
- To start the graphical surface directly from the Raspberry Pi: type 'startx' in the console

2.5.2 Starting the Raspberry Pi and some useful Commands

- It is easier to work with the Raspberry Pi using a SSH client like MobaXterm [33].
- To start the graphical surface in MobaXterm type 'startlxde' in the console.
- The main folder for the readout of the pressure is \oversight.
- To add new sensors go into \oversight\code\oversight\sensors and add a new class there by writing a new Python code (e.g. pressure.py, MCP3008.py). The codes are described in detail in the appendix B.4 and B.2.
- When adding/changing sensors the homepage has to be restarted. Open the Linux terminal: `sudo supervisorctl restart oversight:*`.

```
pi@raspberrypi / $ sudo supervisorctl restart oversight:*
www: stopped
sensor: stopped
www: started
sensor: started
pi@raspberrypi / $
```

Figure 2.15: Restart oversight.

- Restarting the nginx server: `sudo service nginx start` OR `sudo systemctl start nginx` (for newer versions).

```
pi@raspberrypi / $ sudo service nginx stop
Stopping nginx: nginx.
pi@raspberrypi / $ sudo service nginx start
Starting nginx: nginx.
pi@raspberrypi / $ sudo service nginx status
[ ok ] nginx is running.
pi@raspberrypi / $
```

Figure 2.16: Restart nginx.

2.5.3 Adding New Sensors

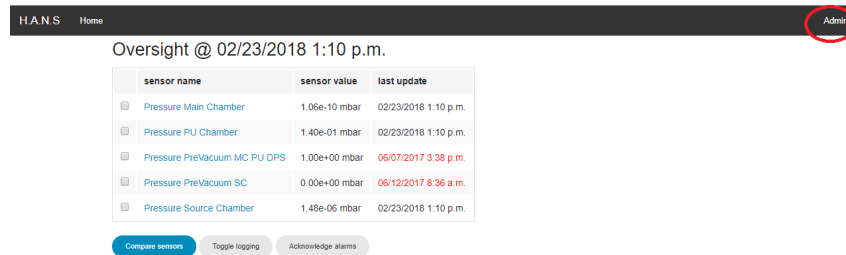
Adding new sensors is done in two steps: In the first step a new class in Python is defined (reason: analogous and digital readouts need different Python codes). In the second step the new created sensor class is added on the homepage. Both steps are described in the following sections.

Adding New Sensor Class in Oversight

On the Raspberry Pi go into \oversight\code\oversight\sensors and add the new sensor class there. At the moment this folder contains two classes of sensors: pressure.py and MCP3008.py (stand: Feb. 2018).

Adding Sensor on Homepage

- Visit <https://fexhrpifslab.tugraz.at/oversight/> and log in as administrator (see figure 2.17). Username and password for the homepage are noted in the OneNote: 01 Miscs/ Raspberry Pi.

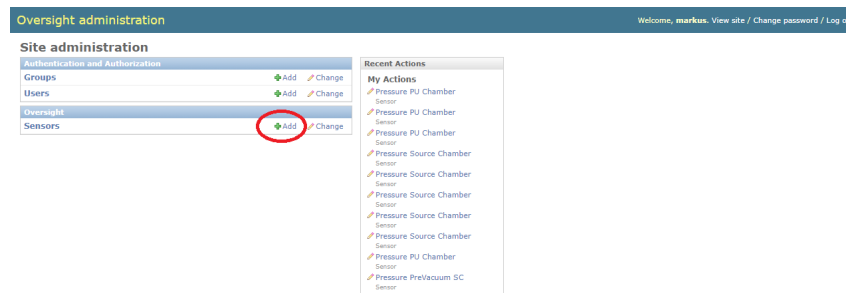


The screenshot shows the Oversight homepage. At the top, there is a navigation bar with 'H.A.N.S.' and 'Home' on the left, and a red circle around the 'Admin' button on the right. Below the navigation bar, the text 'Oversight @ 02/23/2018 1:10 p.m.' is displayed. A table lists several sensors with their names, values, and last update times. Below the table, there are three buttons: 'Compute sensors', 'Toggle logging', and 'Acknowledge alarms'.

sensor name	sensor value	last update
<input type="checkbox"/> Pressure Main Chamber	1.06e-10 mbar	02/23/2018 1:10 p.m.
<input type="checkbox"/> Pressure PU Chamber	1.40e-01 mbar	02/23/2018 1:10 p.m.
<input type="checkbox"/> Pressure PreVacuum MC PU DPS	1.00e+00 mbar	06/07/2017 3:38 p.m.
<input type="checkbox"/> Pressure PreVacuum SC	0.00e+00 mbar	06/12/2017 8:36 a.m.
<input type="checkbox"/> Pressure Source Chamber	1.48e-06 mbar	02/23/2018 1:10 p.m.

Figure 2.17: Homepage oversight in general.

- Click 'add' on the administration side (see figure 2.18).



The screenshot shows the Oversight administration page. The top bar is blue and contains the text 'Oversight administration' and 'Welcome, markus. View site / Change password / Log out'. Below the bar, there is a 'Site administration' section with a table of links. The 'Sensors' link is circled in red. To the right of the table, there is a 'Recent Actions' section with a list of actions.

Site administration
Administration and Authentication
Groups Add Change
Users Add Change
Oversight
Sensors Add Change

Figure 2.18: Administration side where sensors can be added.

- Add the new sensor by filling the following fields (figure 2.19) and press 'save':
 - Name: name of the new sensor
 - Api endpoint: automatically generated
 - Unit: Unit of measured observable
 - Sensor class: class of the sensor
 - Params: Port and serial command which sensor is read out; depends on sensor class

2 Experimental

The screenshot shows the 'Oversight administration' interface. At the top, there's a header with 'Welcome, markus. View site / Change password / Log out'. Below the header, a breadcrumb trail reads 'Home > Oversight > Sensors > Pressure PU Chamber'. The main section is titled 'Change sensor' and contains a form with the following fields:

- Name:** Pressure PU Chamber
- Api endpoint:** pressure-pu-chamber
- Unit:** mbar
- Sensor class:** oversight.sensors.pressure.PressureSer
- Params:** [{"port": "/dev/ttyUSB2", "sensor": "R1"}]

Below the form, there are several checkboxes:

- ☒ Log plot
- ☒ Logging enabled
- Alarm below: [empty field]
- Alarm above: [empty field]
- ☒ Alarm acked

At the bottom of the form, there are three buttons: 'Delete' (with a red star icon), 'Save as new', and 'Save and continue editing'. The 'Save' button is circled in red.

Figure 2.19: How to add sensor.

- Click on a sensor at the main homepage [34] to see the logged data (figure 2.20).

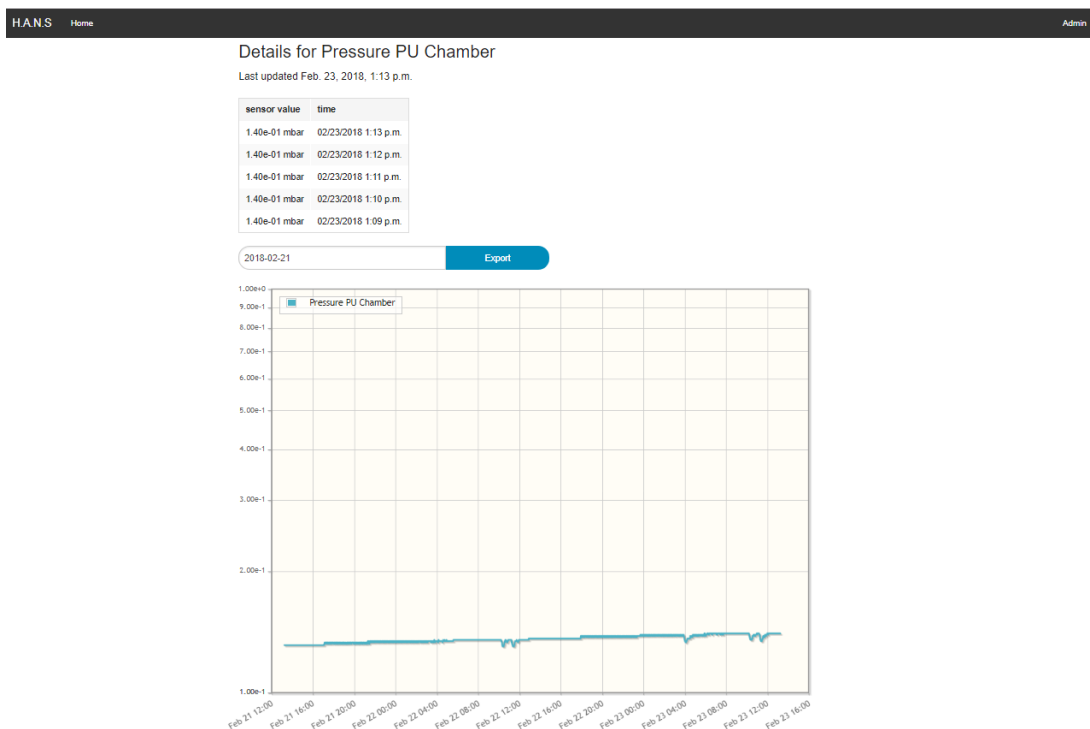


Figure 2.20: Example for a pressure readout.

2.5.4 New Server Certificate

The licence of the homepage server times out after two years and has to be renewed.

- Visit the HeSurfer wiki [35].
 - user: fslab
 - pw: fslab_0815
- At 'Order a SSL certificate' everything is explained, but it is more complicated, so here is a detailed instruction:
 1. Go to <https://www.digicert.com/easy-csr/openssl.htm>.
 2. Fill out the fields shown in figure 2.21.

Certificate Details	Information
Common Name: <input type="text" value="fexphrpifslab.tugraz.at"/> Organization: <input type="text" value="Technische Universität Graz"/> Department: <input type="text" value="Institute of Experimental Physics"/> City: <input type="text" value="Graz"/> State / Province: <input type="text" value="Styria"/> Country: <input type="text" value="Austria"/> Key Size: <input type="text" value="RSA 2048 (recommended)"/> <input type="button" value="Generate"/>	<p>Now just copy and paste this command into a terminal session on your server. Your CSR will be written to fexphrpifslab_tugraz_at.csr.</p> <pre>openssl req -new -newkey rsa:2048 -nodes -out fexphrpifslab_tugraz_at.csr -keyout fexphrpifslab_tugraz_at.key -subj "/C=AT/ST=Styria/L=Graz/O=Technische Universität Graz/OU=Institute of Experimental Physics/CN=fexphrpifslab.tugraz.at"</pre>

Figure 2.21: Server certificate.

3. Click 'Generate'; the key in the right field has to be copied into the Raspberry Pi command line, while being in some folder where one wants to add (temporarily) the .csr- and .key- file. The .csr file is the certificate request, which has to be approved by the ZID (Zentraler Informatik Dienst). The .key file is needed to decrypt the crypted .crt file afterwards.

4. Go to <https://security.tugraz.at/zertifikate/ssl/> → 'Bestellung' and 'Order now'.
5. Upload (or paste the text) of the .csr file in the 'Paste your CSR' section.

Paste your CSR

Click to upload a CSR or paste one

-----BEGIN CERTIFICATE REQUEST-----
MIIChjCCASICAgAwQoCAB7BgWBRATTAFTOMRw=OQYFVQQIGARISB1yaME=OTAL
hg7tLmLRKqY7Yn=J+alagvTfBaMBLlV3haaSTy+amgTmgTgmduydl11e+PzqkGg
R3ZhaJEqMGQSAITEC=whPPEs.dS116XRn11G9MeITV4dPyw11b0x8bCBQaR1+aPRr
NSAaeIYTVOQDOR8onIX=aR7waIf+oGLo8Li37ha1ShdDOCAISI+OQY7XGz11v+h
aGBRKCQahgYgaACCaCcCgYEBABS=yF6u8ba408301=COUaL+nbeCOVFQGT11F
t+vstUnt=Dhv/JL6PST708ZFLa8mas8AQaPha13mhICTc74PWSFig48fy3IEBRK
LPe47QIDBJ/PQURHETImefZLRFX3PambSp73XKac/CaJ=vD011Wa765+hde
7a3BRFT42p+ade7wb7Ej/nuboa+8htCT4GSP+p3+oLUGSp11FOSSAIIVT5Npua11
hguka+veCaagMLPt=8X7wa057QGw7OX184aoSF/cdot+s7y203182e/XRyPl3wY33
Gl8KobJ111//N/qdDRFXT0v=IRF72abBS3=CfyGRhpXTCa=AAaAAAAGAGOCGQC
81a3DQ8EC=DAa18a2Ga8aafSG2yEDU14yQTNa7ay18dy7amDSaH=7pa0xJ5amp

What does a CSR look like?

How do you generate a CSR?

To remain secure, certificates must use keys which are at least 2048 bits in length.

Common Name

+Show Recently Created Domains

fexphrpifslab.tugraz.at

Other Hostnames (SANs)

Optional

OPTIONAL

Organization

Secure Information Technology Center - Austria

Organization Unit

Institute of Experimental Physics

Validity Period

☐ 1 Year

☒ 2 Years

Signature Hash

SHA-256

Figure 2.22: Example for csr.

6. Make sure that new validity is two years.
7. Fill out name, mail, comment to admin (e.g. group name: Markus Koch Group).
8. After about two days a .crt or .pem files should be sent by the ZID . Paste this file and the key file in the folder '/etc/nginx/ssl on the Raspberry Pi and rename those files to: 'fexphrpifslab__tugraz.at.key' and 'fexphrpifslab__tugraz.at.pem'. Replace the old files if necessary.
9. The homepage is ready again.

CHAPTER 3

Characterisation Measurements

In chapter 2 the whole experimental setup is described. Before we were able to start successful measurements some characteristic measurements to improve energy resolution and temporal resolution had to be performed. In this chapter the results of both characterisation measurements is presented.

The energy resolution is optimized by changing the repeller voltage. This affects the electron spectrum in a very positive way: The photoelectron peak changed from one broad peak to the three peaks of the 3p acetone Rydberg states.

The temporal resolution was increased using the prism compressor. After the first measurement with bad temporal resolution it was observed that the $3p_x$ state is doing something weird after the overlap. To figure out which effect happens after the overlap, a better temporal resolution was needed. ter Steege et al. [7] already discovered vibronic coupling between the $3p_x$ and $3p_y$ state. Observing the same effect is a proof that the prism compressor is able to improve the temporal resolution and furthermore, that the theory of vibronic coupling can be reproduced in our experiment. An instruction how to measure the cross-correlation with the prism compressor is described in chapter 3.2.

3.1 Energy Resolution

The basic problem with the energy resolution was already shown in chapter 2.1.3: The energy resolution of the TOF spectrometer strongly depends on the repeller voltage. By applying more positive voltages on the repeller we are able to improve the energy resolution due to the longer flight time of the electrons in the TOF spectrometer.

The energy resolution is adjusted in the following way:

- Set repeller to low z-position (away from the ionization region).
- Take an PE spectrum at 200 fs.
- Look, if the peaks of the 3p Rydberg states are observable. Of course, this depends on the chosen wavelength. Here a wavelength of 333 nm was chosen which is the direct population of the $3p_y$ state. Due to the fact that the bandwidth of the pump pulse is about 80 meV the peaks of $3p_x$ and $3p_z$ should also be visible (see figure 4.1).
- Take a PE spectrum at 200 fs for different repeller voltages again and choose the best.

Figure 3.1 demonstrates the change of the PE spectrum for different repeller voltages. The shift of the peaks to the left side at higher voltages is due to the decrease of the kinetic energy of the electrons. As one can see at higher positive repeller voltages the energy resolution becomes a lot better, observable in the change of one broad peak starting at 0 V to three peaks at 0.6 V-1.3 V. These peaks indicate the 3p Rydberg states of acetone. The theoretical values of the states were measured with synchrotron radiation and it was observed that the spacing between $3p_x$ and $3p_y$ is 40 meV, between $3p_y$ and $3p_z$ it is 50 meV [8] (shown in figure 4.1). Figure 3.1 also shows, that at 1.4 V the energy resolution is going to decrease again. The spectra in figure 3.1 were taken later with 336 nm excitation wavelength.

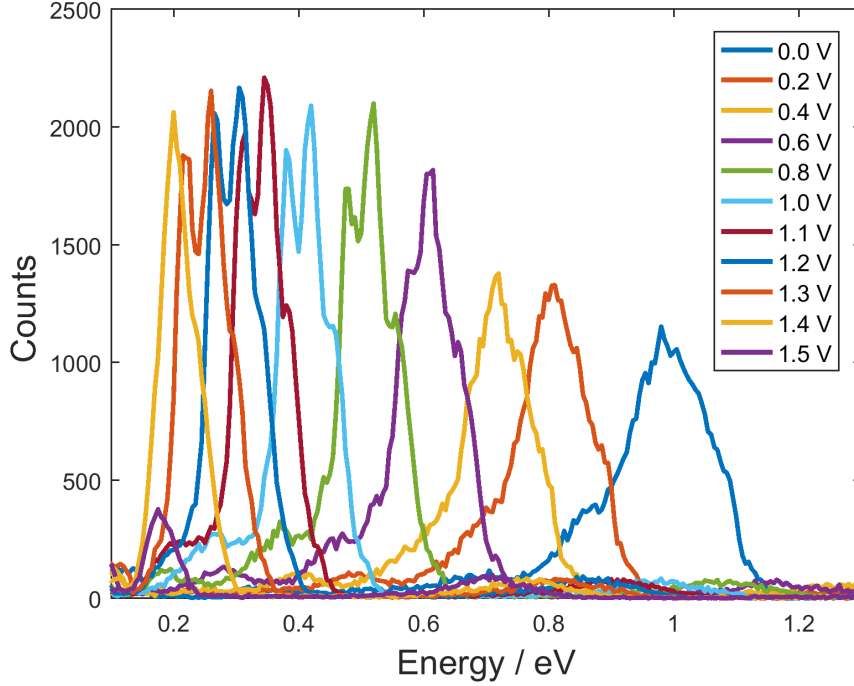


Figure 3.1: PE spectra for different repeller voltages. The improvement of the energy resolution is clearly observable for higher positive repeller voltages. At some voltage the signal drops. Pump wavelength: 336 nm, probe wavelength: 401 nm. Measurement date: 08.02.2018

Figure 3.3 shows the dependence of total counts versus repeller voltage. As written above at 1.4 V repeller voltage the electrons do not have enough kinetic energy to hit the MCP which results in a drop of the total signal. Furthermore, it was observed that after 4.5 μ s no electron signal is recorded.

In this experiment the repeller voltage was set to 1.1 V to be on the safe side. Figure 3.2 compares the peak shapes of a bad and good energy resolution. The electron spectrum recorded with 0.0 V repeller voltage shows a broad peak. The orange plot was taken with 1.1 V repeller voltage. According to the energies of the 3p Rydberg states [8] the left peak at 0.30 eV indicates the $3p_x$ state, the middle peak at 0.35 eV is $3p_y$ and right peak at 0.39 eV shows the $3p_z$ state. The original peak, taken with 0.0 V repeller voltage, was shifted from the spectrum in figure 3.1 to demonstrate the transition to better energy resolutions.

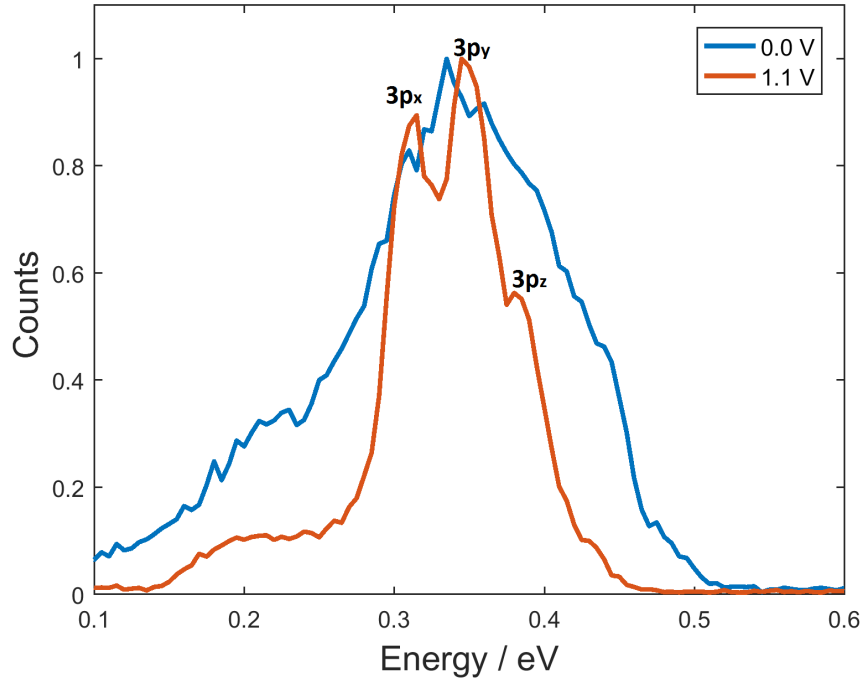


Figure 3.2: Comparison of two peaks with 0.0 V and 1.1 V repeller voltage. Orange spectrum: left peak: $3p_x$, middle peak: $3p_y$, right peak: $3p_z$.

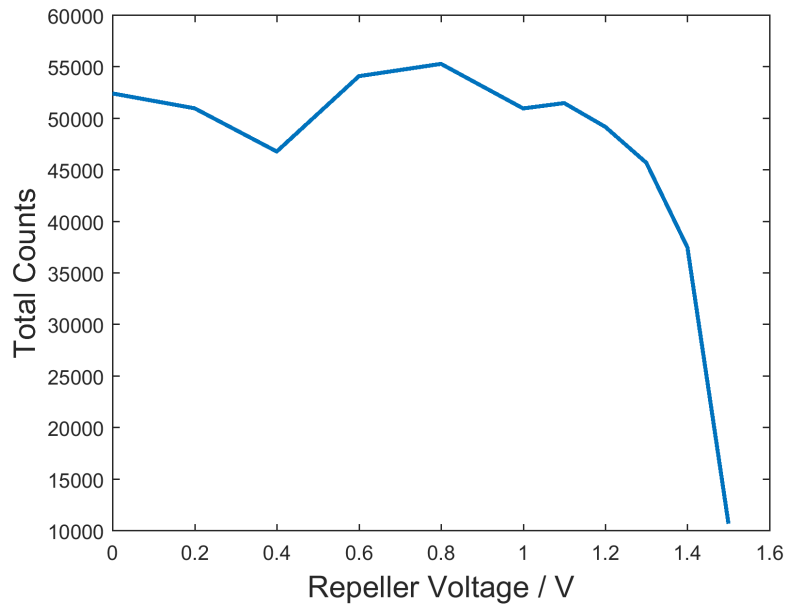


Figure 3.3: Total counts over repeller voltage. At some point the electrons do not have enough kinetic energy to hit the detector which will result in a drop of the signal.

Finally, it should be mentioned that the absolute value of the repeller voltage also depends on the position of the repeller. At the moment the repeller lies at low z -positions. A z -position scan was already done in the master's thesis of Markus Bainschab [22].

3.2 Temporal Resolution

The second improvement was the implementation of a prism compressor. The working principle is described in chapter 3.2. This section is going to show how the cross-correlation looks like and which conclusions we obtain from it.

The measurement of the cross-correlation is performed with xenon gas at a pressure of $4 \cdot 10^{-6}$ mbar. Due to the fact that there is no state excited no dynamics are observed. This makes xenon a perfect tool to check the real cross-correlation.

Because the ionization potential of xenon lies at 12.7 eV, as shown in figure 3.4, three pump photons and one probe photons are needed to ionize the atom directly. Furthermore, the signal is proportional to I^N , where I is the intensity and N is the number of photons. Therefore, the diameter of the beams should be small to be able to measure cross-correlations.

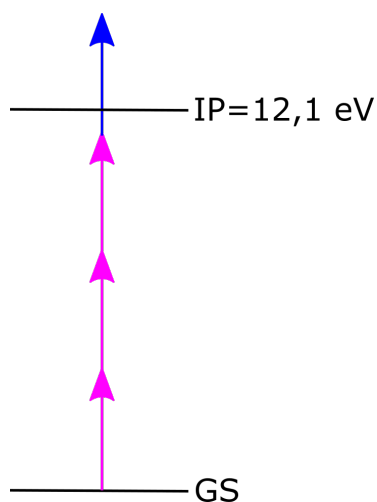


Figure 3.4: Ionization potential for xenon. Three pump photon and one probe photons are used to ionize the atom. Pump wavelength: 333 nm , probe wavelength: 405 nm

How the cross-correlation of xenon looks like is demonstrated in figure 3.5 and figure 3.6. The low signal on the left and the right side of the cross-correlation is the sum of pump only and probe only. The signal is the highest when pump and probe pulse overlap at their time zero. Both spectra are measured with ions, because of their different masses xenon can be separated from remaining acetone in the chamber.

The temporal resolution is measured in the following way:

- Change the gas to xenon at a pressure of $2 \cdot 10^{-6}$ mbar.
- Apply 2 kV to detect ions (attention: set new gates on the counter, because xenon has a different atomic mass than acetone).
- Perform a cross-correlation scan with xenon.
- If the cross-correlation is too high as in figure 3.5. change the distance of both prism to three points: maximum / middle / minimum distance with respect to the door.
- Do a cross-correlation scan again at every of those points.
- If the cross-correlation is smaller than 100 fs as, for example in figure 3.6, switch back to acetone and start the measurement.

The cross-correlation in figure 3.5 is about 100 fs but for this experiment a cross-correlation smaller than 100 fs is needed. Different prism compressor configurations were tested till the temporal resolution was improved.

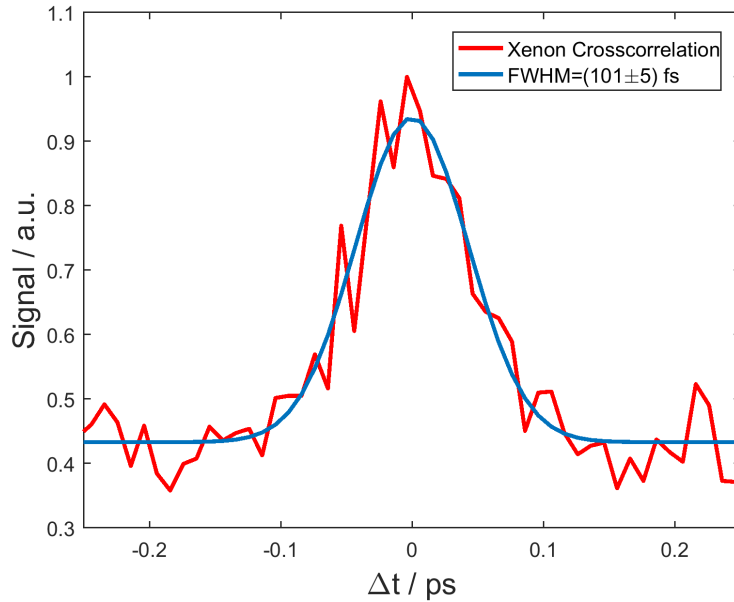


Figure 3.5: Example of a bad cross-correlation. The temporal resolution is about 100 fs.
Pump wavelength: 333 nm , probe wavelength: 405 nm.
Measurement date: 04.01.2018, time scan number: 1126

If the prism compressor is well adjusted, the cross-correlation can be reduced to $\tau_{\text{measured}}=77$ fs as demonstrated in figure 3.6, which allows to resolve the vibronic coupling of the $3p_x$ state with $3p_y$ [7].

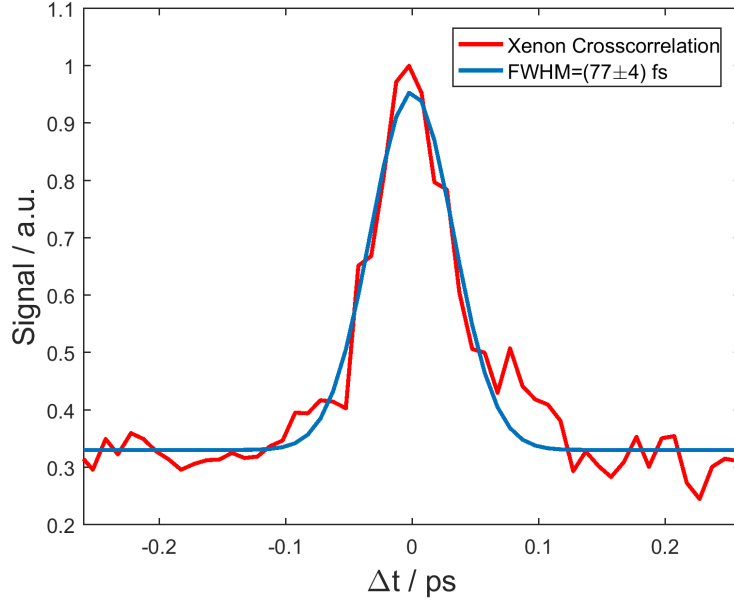


Figure 3.6: Better cross-correlation with a width of 77 fs. This cross-correlation is used in our experiment to make vibronic coupling visible. Pump wavelength: 333 nm, probe wavelength: 405 nm.
Measurement date: 04.01.2018, time scan number: 1130

Another interesting question is how the transform limited cross-correlation for every crystal looks like. Table 2.1 lists the transform limits for all SHG crystals. The cross-correlation can be calculated online [36] using the time-bandwidth product: $\Delta E \cdot \Delta \tau = \text{const.}$ The transform limited pulse of the OPA τ_{OPA} was calculated using the spectrum 434 (measurement date: 03.01.2018, 1000 μm SHG crystal): $\tau_{\text{OPA}}=26$ fs.

The shortest cross-correlation τ_{theor} for different transform limited SHG crystals τ_{SHG} is calculated with $\tau_{\text{theor}} = \sqrt{\tau_{\text{OPA}}^2 + \tau_{\text{SHG}}^2}$ and shown in table 3.1.

The cross-correlation in figure 3.6 was measured with the 1000 μm crystal and is in good agreement with the theoretical calculation: $\tau_{\text{measured}}=77$ fs; $\tau_{\text{theor}}=76$ fs. There are still some simplifications because the order of the non-linear process is not known when doing our cross-correlation measurements.

The gating compressor influences the pulse duration of OPA and SHG path. For the cross-correlation measurement in figure 3.6 it was observed that the chirp configuration where the OPA had the most output power also gave the maximum output power in the SHG path. While it is hard to say if the OPA has the shortest pulse duration with this chirp configuration, the pulse created from the SHG crystal should be transform limited at

maximum output power. At maximum SHG output power the most energy of the 800 nm red light is converted in the non-linear process into the blue light. In order to see how the true transform limited OPA pulse looks like, a measurement with our SD-FROG [37],[23] for different prism compressor configurations was performed. Unfortunately, OPA power fluctuations did not allow to do a successful measurement at this time. As consequence the theoretical cross-correlation using the 1000 μm crystal is the most trustable at the moment. The influence of the chirp at maximum OPA output power to the SHG output power was never tested for other crystals before.

As a suggestion the pulse duration of the SHG pulse could also be manipulated by building glass wedges [38] into the beam path.

Table 3.1: Theoretical cross-correlations

$l \cdots$ length of the crystal

$\tau_{\text{SHG}} \cdots$ transformlimit of SHG crystal

$\tau_{\text{OPA}} \cdots$ transformlimit of OPA

$\tau_{\text{theor}} \cdots$ theoretical transform limited cross-correlation

$l / \mu\text{m}$	$\tau_{\text{SHG}} / \text{fs}$	$\tau_{\text{OPA}} / \text{fs}$	$\tau_{\text{theor}} / \text{fs}$
100	29	26	39
200	37	26	45
500	56	26	62
1000	71	26	76
5000	195	26	197

To sum everything up in this chapter doing successful measurements is only possible when energy resolution and temporal resolution were able to improve. The energy resolution is important because the $3p_x$, $3p_y$ and $3p_z$ state of acetone lie close together. Furthermore, the $3p_x$ state has vibronic coupling with the $3p_y$ state which is only observable if the temporal resolution is good enough. Both could be done and is a huge step forward on the experimental side due to the fact that the He_N droplet experiment benefits from this new knowledge too.

The evaluation of the PE spectra together with their interpretation is presented in the chapter 4.

CHAPTER 4

Results

Here the results of the measurements on acetone molecules in gas phase and their temporary interpretation are presented.

The goal of this master's thesis was on the one hand the extension of the experimental setup and on the other hand the direct excitation of 3p Rydberg states in acetone. In our latest acetone paper [12] high lying Rydberg states were excited using more pump intensity. We observed an indirect filling of 3p states by internal conversion (IC), meaning there was population transfer from those high Rydberg states to the 3p states, however, the energy resolution was limited due to the fact that PEPICO measurements were performed. Furthermore, as presented in figure 4.1 the 3p states are additionally, split up into three states, namely $3p_x$, $3p_y$ and $3p_z$ with their own symmetries A_2 , A_1 , B_2 , respectively. Because Rydberg states are molecular orbitals with atomic character they have different symmetries [4].

The whole experiment is in cooperation with the theoretical group of Prof. Leticia Gonz  les (University of Vienna), who simulated the potential energy surfaces for those Rydberg states and, in addition, they calculated the decay time constants for each state. The theoretical simulations figured out that the time constants are symmetry dependent, so the population of each states decays different fast according to the symmetries of each state.

The current experiment is still in process and following pump wavelengths were chosen (black values on the y-axis in figure 4.1): 336 nm, 333 nm, 329 nm, 324 nm, 320 nm. The wavelength of the probe pulse was always 401 nm.

This master's thesis shows the result and interpretation of 333 nm excitation energy, which

follows the direct excitation of the $3p_y$ state. $3p_y$ lies between $3p_x$ and $3p_z$ as indicated in figure 4.1.

4.1 3p Rydberg State Energies and Symmetries

Starting with the description of the results it is necessary to understand why a variation of pump wavelengths was done. Figure 4.1 demonstrates the potential energy surface of the 3p Rydberg states for the C=O-stretch reaction coordinate. These states are parallel with the result that electronic excitations in one state will also excite vibrational levels of different electronic states.

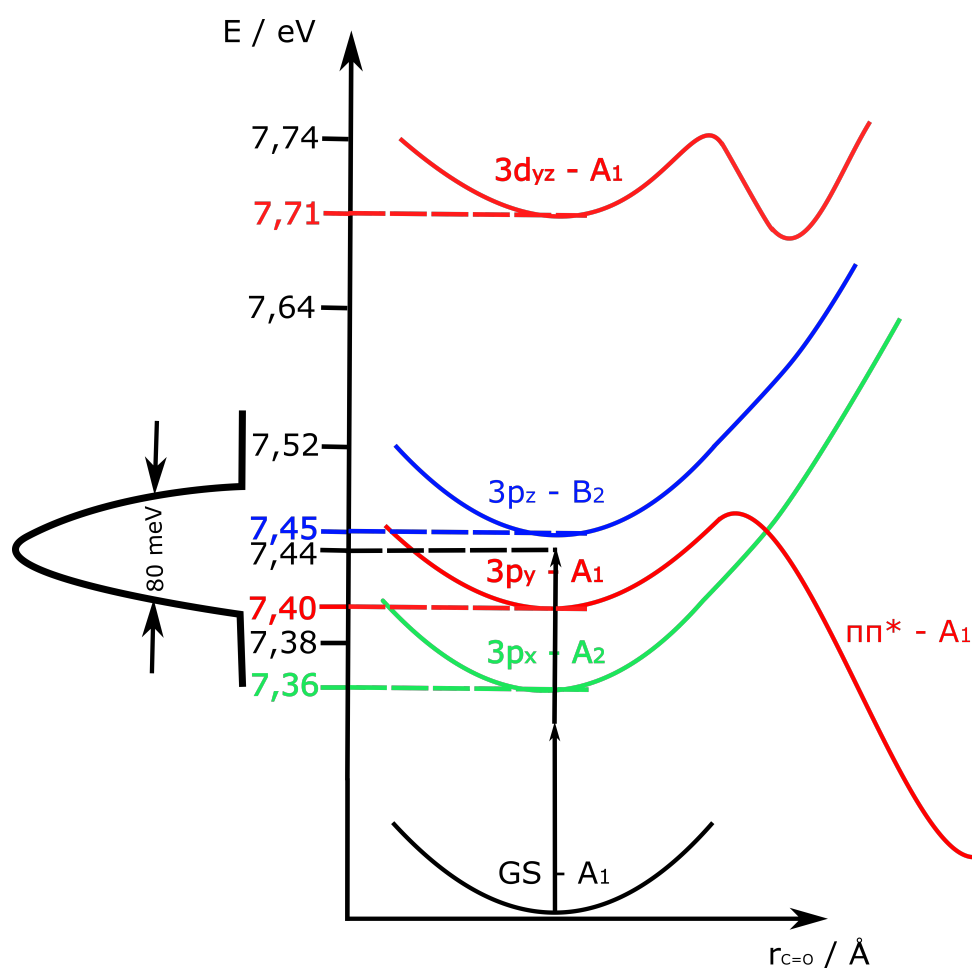


Figure 4.1: The potential energy of different states in acetone in the C=O stretch reaction coordinate. The green, red and blue values on the y-axis indicate the synchrotron measurements [8]. The black values are our chosen wavelengths. The black dashed line shows the excitation energy in the current experiment. The OPA pulse has a bandwidth of 80 meV.

As always the ground state has the highest symmetry A_1 . By taking a closer look to the

3p states of acetone, one can see that there are three states: $3p_x$, $3p_y$ and $3p_z$. Every single state has different symmetry. The $3p_y$ state couples with the valence state $\pi\pi^*$ because both have same the symmetry A_1 . The coupling also leads to an avoided crossing, indicated as a double minimum structure, as suggested with the $3d_{yz}$ state.

The theory group of Prof. Letica Gonz  les (University of Vienna) calculated the decay time constants for each of these 3p states using their new program code 'SHARC' (surface hopping including arbitrary couplings)[19]. They expect these time constants to be different due to the different symmetries of the states. Table 4.1 lists the calculated values of the time constants. $3p_y$ has A_1 symmetry and decays the fastest compared to $3p_x$ and $3p_z$ due to the coupling with $\pi\pi^*$. They also got slightly different values for the energy levels of the 3p states (see table 4.1), but for our experiment we took the values from the synchrotron measurements [8].

The main goal was now to create a working setup and proof if the theoretical prediction is right.

Table 4.1: Calculated time constants from theory

State ... name of the excited state
 τ ... time constant of the state
Err ... error of the time constant
Sym ... symmetry of the states
 E ... energy level of each state

State	τ / fs	Err / %	Sym	E / eV
$3p_x$	243	22	A2	7.34
$3p_y$	118	38	A1	7.43
$3p_z$	230	23	B2	7.45

4.2 Direct Excitation of the $3p_y$ Rydberg State

In this experiment the $3p_y$ state was excited directly, so a pump wavelength of $\lambda=333$ nm (3.72 eV, 2 photon excitation) and a probe wavelength $\lambda=401$ nm (3.09 eV, 1 photon ionization) were chosen. The temporal resolution was reduced to 77 fs using the prism compressor. The $3p_y$ state lies between $3p_x$ and $3p_z$, so as a result three different peaks in the PE spectra are observed due to two facts:

- The OPA bandwidth is 80 meV (see figure 4.1) and therefore higher than the distance between the 3p states (50 meV, measured with synchrotron radiation [8]).
- The excitation to the vibrational ground state of $3p_y$ will also excite some high vibrational levels of $3p_x$ due to of their parallel character.

For the measurement routine a new MatLab code called 'pumpprobe_various_dt' (see appendix D.1) was written.

This script takes electron spectra at given time delays. The evaluation of the spectra is done in the following way:

- First an electron spectrum at some time delay (here at 130 ps) is chosen where all three peaks of the 3p states are clearly resolved (see figure 4.2).

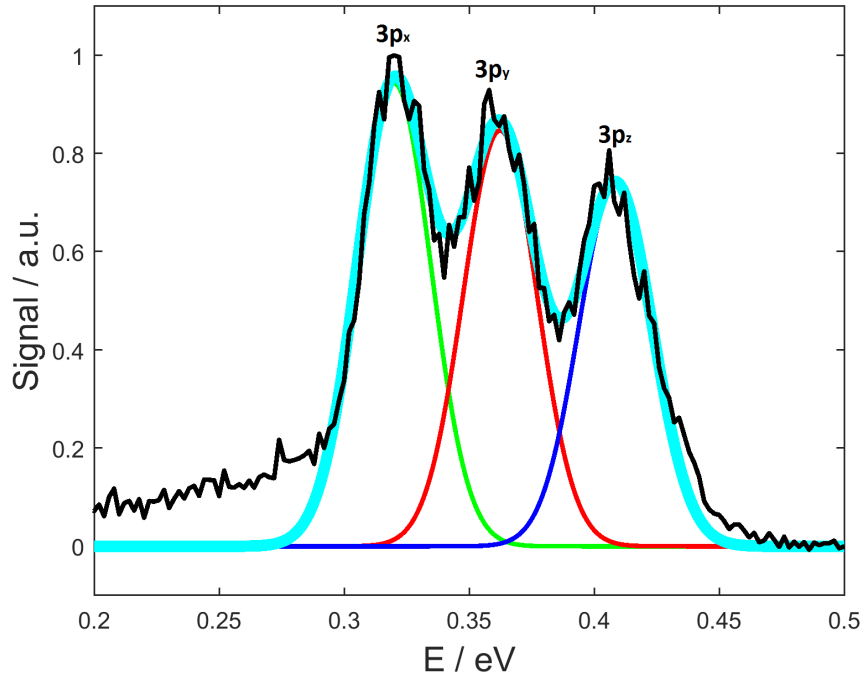


Figure 4.2: Evaluation of the PE peaks by fitting a combination of three Gaussian peaks into it. The black curve is the PE spectrum including the three peaks of the three states. The cyan curve indicates the fit model, in contrast, green, red and blue curves are the single Gaussian fits for every peak.
Measurement date: 24.10.2017

- Then a fit function which sums three Gaussian (cyan function in figure 4.2) is added:

$$a \cdot \exp\left(-\frac{(E-e_1)^2}{\sigma_1^2}\right) + b \cdot \exp\left(-\frac{(E-e_2)^2}{\sigma_2^2}\right) + c \cdot \exp\left(-\frac{(E-e_3)^2}{\sigma_3^2}\right)$$
and a first fit is performed, where the fit parameters amplitudes (a , b , c), relative positions of the Gaussians (e_1 , e_2 , e_3) and standard deviations (σ_1 , σ_2 , σ_3) are not fixed.
- If the Gaussian function converges every fit parameter is fixed except of the amplitude (see figure 4.2).
- To continue, every amplitude is fitted in every PE spectra (see figure 4.3).

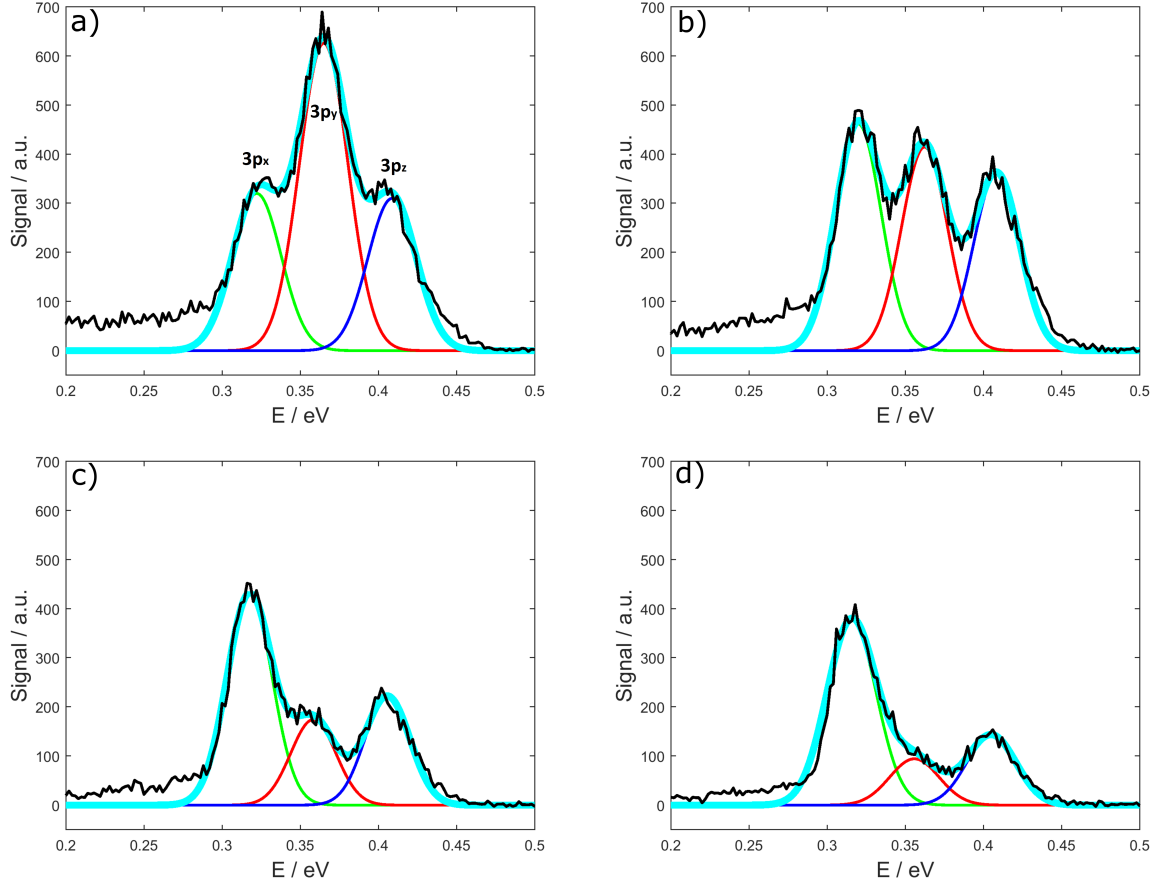


Figure 4.3: PE spectra for different time delays: a) 0 fs, b) 130 fs, c) 300 fs, d) 500 fs.
Measurement date: 24.10.2017

- Finally, the amplitudes from the fit are plotted versus time delay (figure 4.4 and figure 4.5).

The PE spectra in figure 4.3 were taken at the following time delays (drawn as black lines in figure 4.4): 0 fs, 130 fs, 300 fs, 500 fs. The signal is not plotted normalized to see the change of the population for each state. Figure a) shows the PE spectrum on the overlap at 0 fs time delay. Although, the three PE peaks, indicating the 3p Rydberg states, are separated visible this spectrum not as good as the one in figure b) (130 ps) to use it for the Gaussian fit model.

As well figure 4.3 shows the temporal behavior of the population in: Starting on the overlap in figure a) the $3p_y$ is dominating compared to $3p_x$ and $3p_z$. After the overlap all states start decaying indicated with the decreasing signal on the y-axis. $3p_x$ decays the slowest, in contrast, the $3p_y$ state has a faster decay time. At 500 fs (figure d)) the amplitude of the $3p_y$ peak is almost not visible anymore. Additionally, figure d) shows that even at longer time delays the $3p_z$ is still separated and good resolvable.

The origin of the small signal in the energy region of 0.2 eV to 0.3 eV was not found.

4.3 Evaluation of the PE Spectra

For the evaluation of the PE spectra result every fitted Gaussian amplitude is plotted for every time delay as shown in figure 4.3. First it was tried to measure the duration of the pump pulse after it passes the prism compressor with the SD-FROG [37]. Unfortunately, the frog traces were not usable. Even if we were not sure what the true pulse duration is, a PE time scan was done to see if maybe some theoretical prediction can be observed and if the Gaussian fit model works correctly for the evaluation of the data.

Finally the idea to measure the cross-correlation directly with xenon gas (see chapter 3.2) allowed us to see the temporal resolution of the setup and to characterize the prism compressor. So the last measurement was done with the optimized prism compressor and demonstrates the improvement compared to the first measurement and the well known effect called 'vibronic coupling' [7] was reproduced.

4.3.1 Measurement with >100 fs Temporal Resolution

The first measurement was done with a not optimized prism compressor, meaning the temporal resolution was >100 fs. Figure 4.4 presents the decay of all 3p states using an excitation wavelength of 333 nm, where every state is normalized to its maximum. Although, it was a first test scan some quantitative informations can be seen:

- $3p_x$, $3p_y$, $3p_z$ states are separated visible.
- Every state decays with different time constant.
- Because the cross-correlation was not measured the 'real' time zero point is not defined.
- $3p_y$ state (red curve) decays the fastest as expected from theory.
- In contrast, the $3p_x$ state (green curve) decays much slower than in theory and additionally, it looks like that the maximum of its overlap (0-400 fs region in figure 4.4) is shifted compared to $3p_y$ and $3p_z$.

With this information it was clear that the experimental setup works. For a better interpretation of the spectra, especially for the region right after the overlap in figure 4.4, a measurement with improved temporal resolution was the next step.

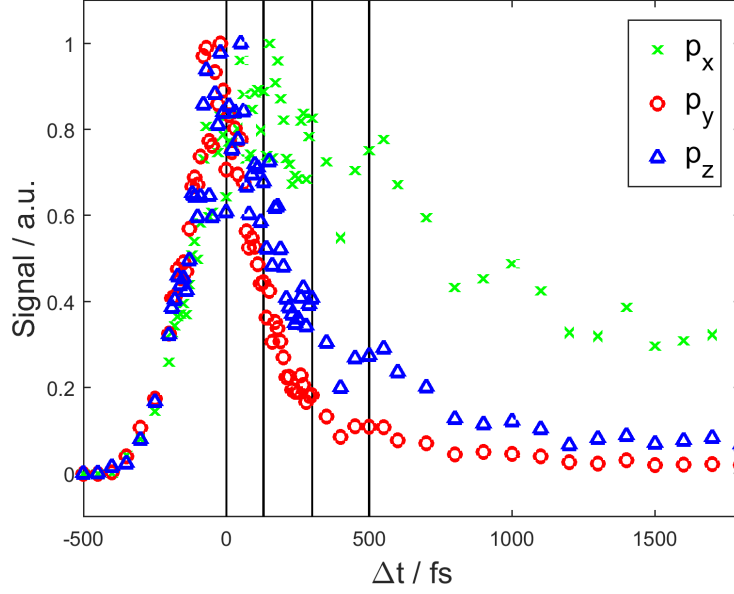


Figure 4.4: Time scan with 333 nm and >100 fs temporal resolution. The three different curves indicate the $3p$ states: green: $3p_x$, red: $3p_y$, blue: $3p_z$. Black lines: PE spectra at different time delays for figure 4.3

Measurement date: 24.10.2017, eiTOF files: 5149-5243

4.3.2 Measurement with 77 fs Temporal Resolution

After adjusting the prism compressor (see chapter 2.4.1) the crosscorrelation was decreased to 77 fs and was measured with xenon (see chapter 3.2) to determine the true time zero point.

In figure 4.5 the fitted amplitudes - $3p_x$, $3p_y$ and $3p_z$ - of the PE spectra are plotted for every time step. Furthermore, the decay time constants for all states is shown in the legend. Figure 4.5 has compared to figure 4.4 a better signal/noise ratio of the $3p_x$ state and the temporal behavior of the $3p_x$ state after the overlap is much better resolved. While in figure 4.5 the maximum of the $3p_y$ and $3p_z$ peak is located at ~ 150 fs the maximum of $3p_x$ appears at ~ 300 fs.

For a first rough estimate the time constants are evaluated by simply using an exponential fit model starting at 400 fs. The $3p_y$ state decays the fastest as expected from theory calculations with (400 ± 30) fs, followed by $3p_z$ with (500 ± 30) fs and $3p_x$ has the slowest decay time with (800 ± 150) fs. However for a full understanding of the filling and decaying process a more advanced fit model has to be used.

The values from theoretical calculations and measurements are compared in table 4.2. Time constants from theory do not match with the fitted ones because in their theoretical calculations they use a semiclassical algorithm: The potential energies are calculated

Table 4.2: Calculated and measured time constants

State ... name of the excited state
 τ_{theory} ... theoretical time constants
 τ_{fit} ... fitted time constants
Sym ... symmetry of the states

State	$\tau_{\text{theory}} / \text{fs}$	$\tau_{\text{fit}} / \text{fs}$	Sym
$3p_x$	243	800	A_2
$3p_y$	118	400	A_1
$3p_z$	230	500	B_2

quantum-mechanically. Afterwards, the travelling behaviour of a sphere is studied in this potentials: At every point of the potential energies the overlap integral is calculated. For the case that two states couple with each other, the overlap integral is non-zero, which is explained as population transfer between those states. A higher starting point on the potential energy lowers the time constants.

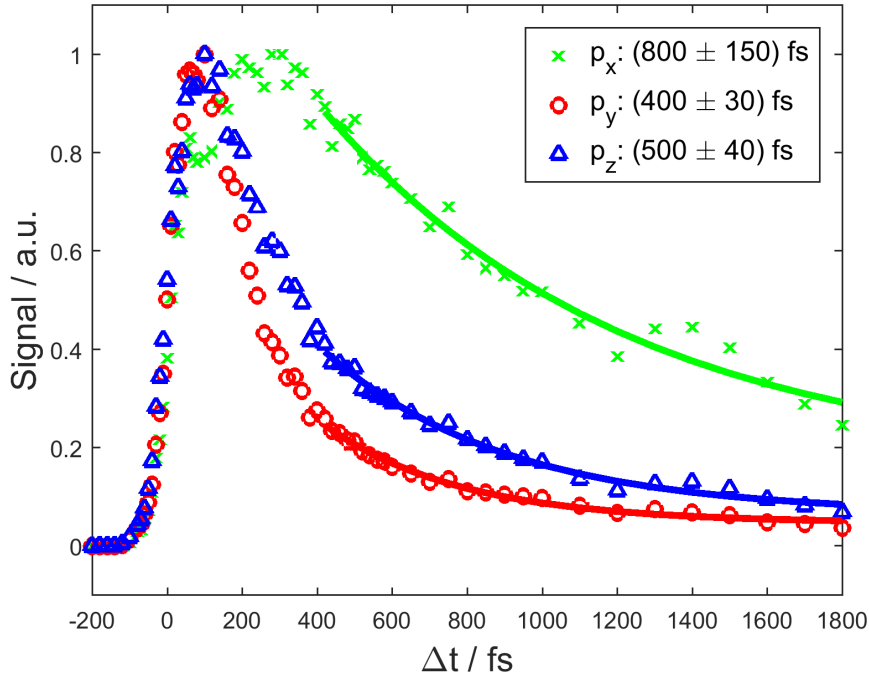


Figure 4.5: Final high resolution time scan at 333 nm and 77 fs temporal resolution. The time constants are fitted using an exponential fit model.

Measurement date: 09.01.2018, eiTOF: 7313-7405

Additional the maximum of the $3p_x$ state is shifted compared to $3p_y$ and $3p_z$, shown detailed in figure 4.6. This was not expected from the theory group because their code does not implement vibrational level and vibronic coupling between the $3p$ states. However,

vibronic coupling of the $3p_x$ state in acetone was already observed [7] and will be described in the next section.

As written above the time constants were calculated with an exponential fit model starting at 400 fs. The exponential fit starts at higher time delays to avoid the influence of the cross-correlation and to guarantee that the time constants are not sophisticated from possible fast relaxation dynamics. To analyse the whole dynamic side a better fit model has to be used.

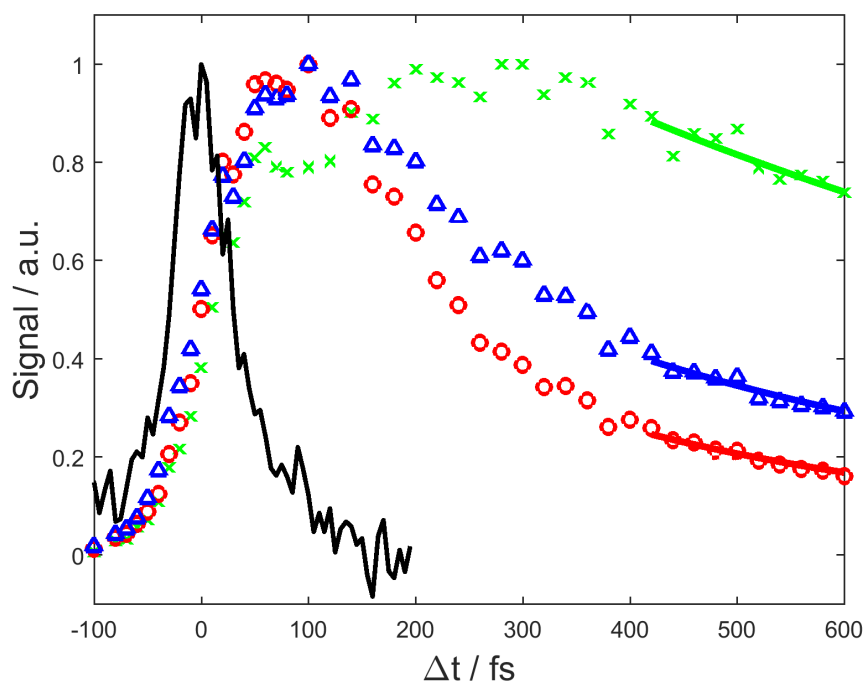


Figure 4.6: Zoomed into overlap region from figure 4.5. In this figure the shift of the maxima of $3p_x$ compared to the other states is visible. In addition the cross-correlation signal with xenon (black curve) is printed to indicate the time zero point of the cross-correlation.

Measurement date: 09.01.2018, eiTOF files: 7313-7405

4.3.3 Vibronic Coupling of the $3p_x$ State

In this section the interpretation of the $3p_x$ maximum shift is described. Figure 4.6 zooms into the overlap region of figure 4.5: The signal of $3p_x$ (green line) is still rising even when $3p_y$ (red line) and $3p_z$ (blue line) are decaying. Population transfer between these states is called 'vibronic coupling' and was already observed by ter Steege et al. [7].

The basics of vibronic coupling is demonstrated in figure 4.7: The symmetry of the whole $3p_x$ electronic state is A_2 . When this state is excited with one vibrational quantum into higher vibrational states (ν_{12x} with a_2 symmetry in figure 4.7) the new symmetry of the electronic state is going to be A_1 (compare symmetries with table 4.3: $A_2 * a_2 = A_1$).

Table 4.3: Product table of C_{2V} pointgroup

$A_1, A_2, B_1, B_2 \dots$ symmetries of the electronic state

$a_1, a_2, b_1, b_2 \dots$ symmetries of the vibrational state

	A_1, a_1	A_2, a_2	B_1, b_1	B_2, b_2
A_1, a_1	A_1	A_2	B_1	B_2
A_2, a_2	A_2	A_1	B_2	B_1
B_1, b_1	B_1	B_2	A_1	A_2
B_2, b_2	B_2	B_1	A_2	A_1

This excited vibrational state of $3p_x$ can couple with the vibronic ground state (ν_{0y}) of $3p_y$, because both electronic states have the same symmetry A_1 now. This leads to population transfers between these states. As result we directly observe the population transfer between the $3p_x$ and $3p_y$ Rydberg state.

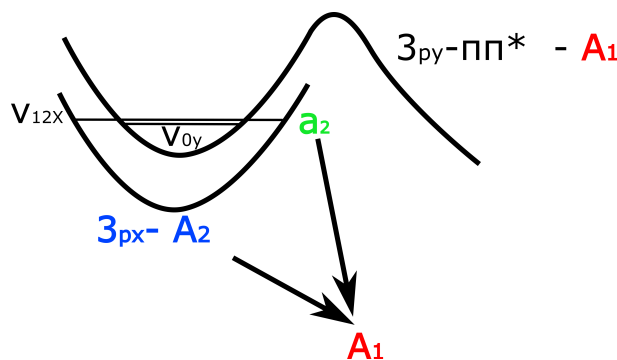


Figure 4.7: Basic example of vibronic coupling. The electronic state and vibrational state have their own different symmetries but in combination the whole symmetry can change.

In summary this is also the reason for the lower time constant of the $3p_y$ because the coupling of $3p_y$ with $\pi\pi^*$ is much stronger due to their same symmetry (A_1) then for the other states and population transfer between those states occurs.

4.4 Summary, Outlook and Open Questions

During the last year we met a lot of challenges starting with the experimental setup and going on with the measurement of the first useful data along with their interpretation.

To begin with the experimental part the summary can be kept short: The setup works well at the moment. OPA and prism compressor are able to be adjusted, as well energy- and temporal resolution are improved.

Surprisingly, the direct excitation of the 3p Rydberg states, using only one wavelength, already showed the expected predictions from theory. The time constant of the $3p_y$ state was lower compared to $3p_x$ and $3p_z$. The well known effect of vibronic coupling could be observed too.

The analysing of the produced data raises some questions which can not be answered completely at the moment mainly, due to the fact that only one excitation wavelength (333 nm) was performed and the whole experiment is still in process. However, the following questions are interesting:

- Do the time constants change for different excitation wavelengths?
- Is vibronic coupling between other states also observable?
- Does a state decay faster if more excitation energy is coupled into the system?

The following experiments are suggested:

- Take PE spectra for the following wavelengths: 336 nm, 329 nm, 324 nm, 320 nm.
- Extend the fit model to describe the filling and decaying process .

CHAPTER 5

Appendix

A Raspberry Pi Hardware

Figure 5.1 shows the pin assignment of the current used Raspberry Pi (described in chapter 2.5). The pressure readout in our laboratory is done by the communication between the Raspberry Pi and our homepage [34]. Additionally we have digital and analogue values for the output voltages of the pressure sensors. Therefore, different Python codes have to be used to read the correct pressure value from each sensor.

The pins can be connected to devices and for the control Python is used. A summary of the pins and their function is described in table 5.1.

Table 5.1: Pins of the Raspberry Pi

Pins	Description	Comment
GPIO	General Purpose Input/Output pin	they can work as input or output pins. Input pins can take the levels HIGH (3.3 V) or LOW (0 V), e.g. from a switch or potentiometer. Output pins can give an output voltage of 3.3 V or 0 V.
GND	Ground	ground lies on 0 V
3.3v	3.3 Volt pin	gives always 3.3 V output
5v	5 Volt pin	gives always 5 V output
ID EEPROM	2 special pins	can be used to attach an ID EEPROM (Electrical Erasable Programmable Read-Only Memory)

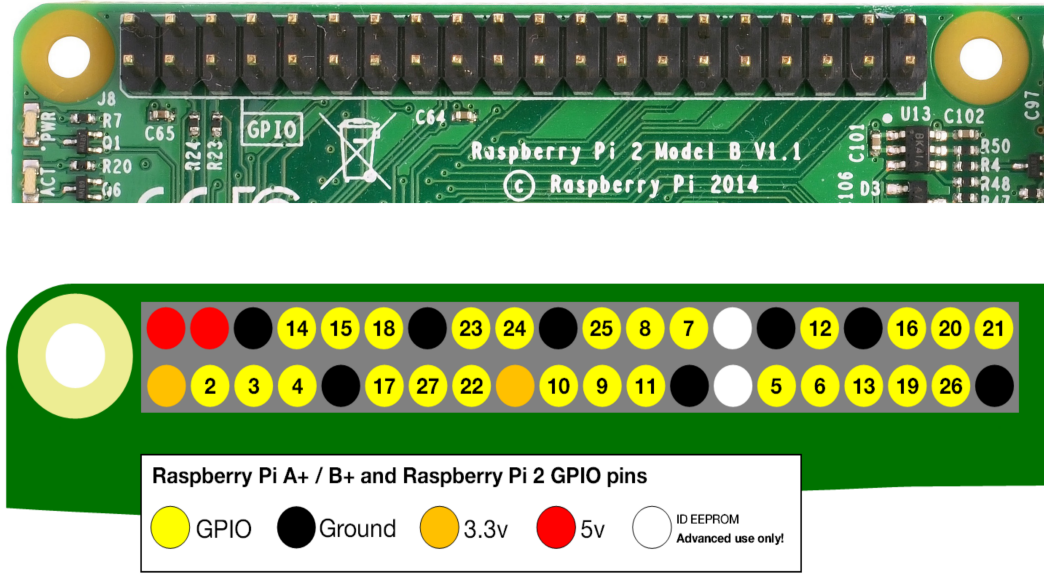


Figure 5.1: Pin assignment of Pi 2 Model B v1.1 [32].

For our application we use these pins to connect an analog to digital converter (ADC), called MCP3008, and furthermore, to read out the pressure of the main chamber connecting a Granville Philipps 350 Ionization Gauge controller to the ADC.

A detailed instruction how to connect the MCP3008 with the Raspberry Pi using 'software SPI' / 'hardware SPI', Library Install / Source Install can be found at [39].

In the appendix of this master's thesis I will summarize the important steps of the homepage and describe the way we use to read out the pressure sensor.

The wiring diagram of the MCP3008 converter is shown in figure 5.2.

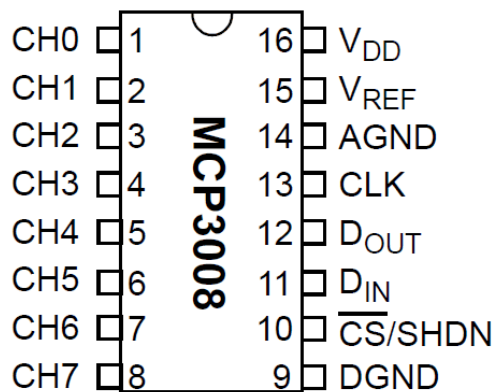


Figure 5.2: Pin assignment of the ADC MCP3008 [39].

'Software SPI' / 'hardware SPI' are two different ways how to connect the MCP3008 with

the Raspberry Pi [39]. For our case the connection was done with 'software SPI'.

- VDD to 3.3 V pin
- VREF to 3.3 V pin
- AGND to GND pin
- DGND to GND pin
- CLK to pin 18
- DOUT to pin 23
- DIN to pin 24
- CS/SHDN to pin 25

Afterwards the 'source install' was done. The full Python code was downloaded from Github as described on the homepage. The testcode 'simpletest.py' is stored in the order /home/pi/Adafruit_Python_MCP3008/examples/simpletest.py on the Raspberry Pi and can be started by typing: 'sudo python simpletest.py' into the terminal. Now the testcode appears in the Python shell as shown in figure 5.3. Simpletest.py is described in B1.

```

pi@raspberrypi: ~/Adafruit_Python_MCP3008/examples
File Edit Tabs Help
pi@raspberrypi ~/Adafruit_Python_MCP3008/examples $ sudo python simpletest.py
Reading MCP3008 values, press Ctrl-C to quit...
 0 | 1 | 2 | 3 | 4 | 5 | 6 | 7 |
-----
3 | 248 | 4 | 5 | 6 | 6 | 13 | 25 |
8 | 249 | 4 | 4 | 2 | 2 | 0 | 1 |
0 | 248 | 1 | 2 | 2 | 2 | 5 | 12 |
7 | 248 | 5 | 6 | 6 | 6 | 13 | 21 |
5 | 250 | 2 | 2 | 1 | 1 | 0 | 0 |
0 | 247 | 3 | 3 | 4 | 4 | 11 | 23 |
9 | 249 | 5 | 5 | 4 | 1 | 0 | 0 |
1 | 249 | 3 | 4 | 5 | 6 | 14 | 25 |
7 | 249 | 4 | 2 | 1 | 0 | 0 | 0 |
3 | 249 | 4 | 6 | 6 | 7 | 12 | 18 |
3 | 248 | 2 | 0 | 1 | 1 | 2 | 11 |
7 | 249 | 6 | 6 | 5 | 4 | 5 | 4 |
0 | 247 | 2 | 2 | 2 | 4 | 10 | 23 |
8 | 248 | 4 | 4 | 3 | 1 | 0 | 0 |
1 | 248 | 3 | 4 | 5 | 7 | 14 | 24 |
7 | 247 | 2 | 2 | 0 | 0 | 0 | 1 |
4 | 248 | 5 | 6 | 7 | 6 | 11 | 16 |
^CTraceback (most recent call last):
  File "simpletest.py", line 39, in <module>
    time.sleep(0.5)

```

Figure 5.3: How to run simpletest.py in the Python terminal.

This figure lists all channels of the MCP3008 with their analogue-digital values. The values present number from 0 to 1023, with 0 as the ground level and 1023 as 3.3 V. In the next step we had to modulate the test code for our application, which will be described in the next section.

B Python Codes

In this section the Python programs which are currently used to read out the pressures will be presented. The readout of the Granville Philipps 350 Ionization Gauge controller is done with an analogue digital converter, as written in the section above. In contrast, the readout of the gauge controller Pfeiffer Vacuum TCP 321 work fully digitalized and therefore different Python codes have to be used.

B.1 simpletest.py

The code 'simpletest.py' can be downloaded from the homepage [39] and demonstrates an example how to read out the analogue digital converter MCP3008 in general. Using this code is basically to test if the wiring from ADC to Rasperry Pi works fine and additionally, if the Python code can be started from the Rasperry Pi.

Because the software SPI configuration was used, the hardware SPI configuration is commented out. 'simpletest.py' generates eight columns and prints the pressure value of each channel. Furthermore, every 0.5 seconds a new row is added including the updated values.

The program can be stopped by pressing 'Ctrl-C' in the terminal.

```
1 # Simple example of reading the MCP3008 analog input channels
2 # and printing
3 # them all out.
4 # Author: Tony DiCola
5 # License: Public Domain
6 import time
7
8 # Import SPI library (for hardware SPI) and MCP3008 library.
9 import Adafruit_GPIO.SPI as SPI
10 import Adafruit_MCP3008
11
12
13 # Software SPI configuration:
14 CLK = 18
15 MISO = 23
16 MOSI = 24
17 CS = 25
18 mcp = Adafruit_MCP3008.MCP3008(clk=CLK, cs=CS, miso=MISO, mosi=MOSI)
19
20 # Hardware SPI configuration:
21 # SPI_PORT = 0
22 # SPI_DEVICE = 0
23 # mcp = Adafruit_MCP3008.MCP3008(spi=SPI.SpiDev(SPI_PORT, SPI_DEVICE))
24
25
26 print('Reading MCP3008 values, press Ctrl-C to quit...')
27 # Print nice channel column headers.
28 print('| {0:>4} | {1:>4} | {2:>4} | {3:>4} | {4:>4} |'
29       '| {5:>4} | {6:>4} | {7:>4} |'.format(*range(8)))
30 print('-' * 57)
```

```
31 # Main program loop.
32 while True:
33     # Read all the ADC channel values in a list.
34     values = [0]*8
35     for i in range(8):
36         # The read_adc function will get the value
37         # of the specified channel (0-7).
38         values[i] = mcp.read_adc(i)
39     # Print the ADC values.
40     print(' | {0:>4} | {1:>4} | {2:>4} | {3:>4}
41           | {4:>4} | {5:>4} | {6:>4} | {7:>4} | '.format(*values))
42     # Pause for half a second.
43     time.sleep(0.5)
```

B.2 MCP3008.py

The code 'simpletest.py' was modified to read out the pressure of the analog gauge controller. The analog value is converted by the formula $10^{(value-10)}$ which is taken from the manual of the sensor.

In the code below the formula has to be modified for Python using $value = 10 * (value / \text{float}(1009) * 3.3 - 10)$. In Python $**$ is the correspondence to \wedge and furthermore, 'float' has to be written in the denominator to do divisions. Otherwise Python performs integer divisions (e.g. $1 / 2$ gives 0). The value '1009' in line 29 are converted from 3.25 V, which was measured for the true output voltage of the sensor.

```
1 # Import SPI library (for hardware SPI) and MCP3008 library.
2 import Adafruit_GPIO.SPI as SPI
3 import Adafruit_MCP3008
4 import time
5 import decimal
6
7 from .base import Sensor
8
9 class MCP3008Sensor(Sensor):
10     def __init__(self):
11         print("init")
12         self.CLK = 18
13         self.MISO = 23
14         self.MOSI = 24
15         self.CS = 25
16         self.sensor = Adafruit_MCP3008.MCP3008(clk=self.CLK,
17         cs=self.CS, miso=self.MISO, mosi=self.MOSI)
18
19     def read(self):
20         print("read")
21         value = self.sensor.read_adc(1)
22         value = 10**((value/float(1009)*3.3-10))
23         return value
24
```

```
25     def to_string(self, value):
26         return '%.2e' % value
27
28     def from_string(self, value):
29         return decimal.Decimal(value)
```

B.3 serial_test_class.py

On the Raspberry Pi a test program is stored in the folder /home/pi/python.

'serial_test_class.py' can be used to ensure that the communication between Raspberry Pi and sensors works correctly, without using one of the codes in the /oversight order. The following code has three variable parameters: port, baudrate (9600, 19200 or 38400) and sensor. If the communication works, the positive ACK '06' is displayed and the value of the pressure is printed.

```
1 import serial
2 import time
3 import decimal
4
5 CR='\r'
6 ENQ='\x05'
7 Res='\x03'
8 sleeptime=0.05
9
10 #care: BAUDRATE = 9600, 19200 or 38400
11
12
13
14 #class Sensor:
15
16 def pressure(port, baudrate, sensor):
17     ser = serial.Serial(port, baudrate, parity=serial.PARITY_NONE,
18     stopbits=serial.STOPBITS_ONE)
19     ser.write(Res+sensor+CR) #first reset the input buffer
20                             #then write to the sensor
21     #ser.write(sensor+CR) #write to the sensor
22     time.sleep(sleeptime)
23     ack=ser.readline() #read acknowledgement -->
24                         #positive ACK gives 06, negative ACK 15
25     #ack=ack[0]
26
27     #to read hex:
28     print ":".join("{:02x}".format(ord(c)) for c in ack)
29     ser.write(ENQ) #write enquirement
30     time.sleep(sleeptime)
31     value=ser.readline().strip()
32     #print ":".join("{:02x}".format(ord(c)) for c in value)
33     dec=decimal.Decimal(value[2:])
34     print('Der Druck betraegt %.2e mbar' %dec)
35     ser.close()
36
37
```



```
38 pressure(port='/dev/ttyUSB1', baudrate=19200, sensor='PR1')
```

B.4 pressure.py

The next code presents the readout for the digital Pfeiffer Vacuum TCP 321 controller. The communication between controller and computer is done with a communication protocol. The full protocol is on page 5 in the Pfeiffer Vacuum manual [40].

Table 5.2 is going to summarize the important commands, helping to understand the following Python codes better. To send commands in Python to the interface use 'write' (e.g. 'ser.write'), for reading use 'readline' (e.g. 'ser.readline').

Table 5.2: Communication commands

Symbol	Meaning	Output Dez / Hex
CR	CARRIAGE RETURN go to beginning of line	3 / 03
ENQ	ENQUIRY request for data transmission	5 / 05
ACK	ACKNOWLEDGE positive report signal	6 / 06
NAK	NEGATIVE ACKNOWLEDGE negative report signal	21 / 15
PR1	measurement data gauge 1	-
PR2	measurement data gauge 2	-

To move on with 'pressure.py' the following code demonstrates the readout of all digital gauge controller using the communication protocol which is described above. The parameters 'port' and 'sensor' are set in the homepage. Another critical part is the correct baudrate. This parameter can be set directly on every gauge controller and has a fix value of 19200 for all controllers at the moment. A sleeptime of 0.05 sec was chosen to make sure no conflicts during the transmission process appear.

```
1 import serial
2 import time
3 import decimal
4
5 from .base import Sensor
6
7
8 CR = '\n'
9 ENQ = '\x05'
10 sleeptime_rs = 0.05
11
12
13 class PressureSensor(Sensor):
```

```
14     def __init__(self, port, sensor):
15         self.port = port
16         self.sensor = sensor
17
18     def read(self):
19         ser = serial.Serial(self.port, 19200, timeout=5,
20                             parity='N', bytesize=8, stopbits=1)
21         ser.write('P'+bytes(self.sensor)+CR)
22         time.sleep(sleeptime_rs)
23         ser.readline() # read acknowledgement
24         time.sleep(sleeptime_rs)
25         ser.write(ENQ) # send enquiry
26         time.sleep(sleeptime_rs)
27         value = ser.readline().strip() # read value
28         ser.close()
29         return self.from_string(value[2:])
30
31     def to_string(self, value):
32         return '%.2e' % value
33
34     def from_string(self, value):
35         return decimal.Decimal(value)
```

C OPA Wavelengths

Figure 5.4 shows the wavelength range of the OPA and how the chosen wavelength is created.

OPeA-Solo User's Manual

Affix 1

Table 5. List of nonlinear crystals for OPeA-Solo

Crystal number	Nonlinear process	Output wavelengths and polarization	Crystal placement	Crystal rotation axis
#1F	S	1160–1600 V	Crystal 1	V
#1	S I	1160–1600 V 1600–2600 H	Crystal 2	V
#2	SHS SHI SFI	580–800 V 800–1200 V 533–600 V	Mixer I	H H H
#5	SH(SHS) SH(SHI)	290–400 H 400–590 H	Mixer II	V V
#6	SH(SFI) SH(SFS)	266.5–300 H 240–266.5 H	Mixer II	V V
#8	DFG1	2600–11000 H	Mixer I	H
#9	DFG2	5000–20000 H	Mixer I	H

- S – Signal
- I – Idler
- SHS – frequency doubling of signal
- SHI – frequency doubling of idler
- SFI – sum frequency generation when mixing pump (800 nm) and idler
- SFS – sum frequency generation when mixing pump (800 nm) and signal
- SH(SHS) – frequency doubling of SHS
- SH(SHI) – frequency doubling of SHI
- SH(SFI) – frequency doubling of SFI
- SH(SFS) – frequency doubling of SFS
- DFG – difference frequency generation when mixing signal and idler pulses

Figure 5.4: The OPA wavelength ranges, extracted from the manual [28].

D Matlab Codes

Here is a summary of the Matlab codes, called 'pumpprobe_various_dt.m' and 'create_eiTOFname.m', which were used for the acetone measurements.

D.1 pumpprobe_varoius_dt.m

This code takes full automatized PE spectra at given timedelays. Furthermore, by setting 'onlynumber=5' after five measurements pump-only and probe-only PE spectra are taken. 'pos0' is the time zero point which has to be determined from the xenon crosscorrelation. Shutter 2 (pump) and Shutter 3 (probe) are controlled by 'PPShutter.m' [23]. Due to the fact that the overlap can shift for long measurements 'sequential' indicates the number of all measurement cycles which are done. If the PE spectra stay constant during one cycle there is a good chance that the produced data can be used.

```
1 function pumpprobe_various_dt()
2     % measure pump probe at various time delays:
3
4     % sequential gives the number of sequences that
5     % shall be taken (i.e. the
6     % number of cycles the whole timescan shall be measured)
7     sequential = 12;
8
9     runs = 1e5;
10
11
12     onlynumber = 5;
13     pos0 = 43.97113;
14     time = ([ -200:20:-80, -70:10:70, 80:20:600, 650:50:1000, ...
15     1100:100:2000, 2300, 2600, 2900]')/1000;
16     time = repmat(time, sequential, 1);
17
18
19     PPShutter('O')
20
21     try
22         for k = 1:numel(time)
23             fprintf('Time: %g\n', time(k))
24             fprintf('Pump Probe\n')
25             abs_move(TimeToPos(time(k), pos0));
26             pause(1)
27             startMeasurement(runs);
28
29             % perform pump/probe onlys:
30             if ~mod(k, onlynumber)
31                 pause(1)
32                 PPShutter('U')
33                 pause(1)
34                 fprintf('Time: %g\n', time(k))
35                 fprintf('Pump Only\n')
36                 startMeasurement(runs);
37
38
39                 pause(1)
40                 PPShutter('R')
41                 pause(1)
42                 fprintf('Time: %g\n', time(k))
```

```

43         fprintf('Probe Only\n')
44         startMeasurement(runs);
45         pause(1)
46         PPS shutter('O')
47     end
48 end
49 catch ME
50     fprintf(2, '\n%s\n\n', ME.message);
51 end
52
53 PPS shutter('P')
54
55 % return
56 % analyse files , save with eTOFplot and subtract with PlotCov_BG
57 onlynumber = 5;
58 eiTOF_numbers = 17614:18789;
59 eiTOF_pumponly = eiTOF_numbers(onlynumber+1:onlynumber+2:end);
60 eiTOF_probeonly = eiTOF_numbers(onlynumber+2:onlynumber+2:end);
61 eiTOF_numbers(onlynumber+1:onlynumber+2:end) = [];
62 eiTOF_numbers(onlynumber+1:onlynumber+1:end) = [];
63
64
65 for k = 1:numel(eiTOF_numbers)
66     fprintf('File number: %g\n',eiTOF_numbers(k))
67     SignalFile = {[eiTOF_numbers(k)]};
68     BackgroundFiles = num2cell([eiTOF_pumponly(ceil(k/5)),...
69     eiTOF_probeonly(ceil(k/5))],2);
70     SignalOnly= 0;
71     SavePlotData = 1;
72     SignalSummation = 0;
73     leg = {};
74
75     filenumber = [eiTOF_numbers(k);...
76     eiTOF_pumponly(ceil(k/5));...
77     eiTOF_probeonly(ceil(k/5))];
78
79     eTOFplot(filenumber);
80
81     Cov_o_Coi_o_El = 3;% 1 for Covariance, 2 for Coincidence ,
82     % 3 for electrons , 4 for electrons diff
83     PlotCov_BG(Cov_o_Coi_o_El,BackgroundFiles,...
84     SignalFile, SignalOnly, SavePlotData,...
85     SignalSummation, leg);
86     close all
87 end
88
89 end
90
91 function startMeasurement(runs)
92     logical = true;
93
94     while logical
95         try
96             RMT_v2(runs);
97             logical = false;

```

```
98         catch ME
99             fprintf(2, '\n%s\n\n', ME.message);
100         end
101     end
102 end
```

D.2 create_eiTOFname.m

Long measurement create a huge amount of data called eiTOF_filename.

'create_eiTOFname.m' generates an excel list which can be directly imported into OneNote.

```
1 % create automatic eiTOF filenames for given timedelays
2
3 function [] = create_eiTOFname(filename, time, startfile, only_number)
4     currpath = cd();
5
6     if nargin == 0
7         filename = 'acetone_3p_321nm.xlsx';
8         sequential = 12;
9         time = ([ -200:20:-80, -70:10:70, 80:20:600, 650:50:1000, ...
10             1100:100:2000, 2300, 2600, 2900]')/1000;
11         time = repmat(time, sequential, 1);
12         startfile = 17614;
13         only_number = 5; %how often are only spectra measured
14     end
15
16     file = zeros(numel(time), 1);
17     file(1) = startfile;
18     temp_var = 0;
19
20     for i = 1:numel(time)
21         temp_var = temp_var + 1;
22         file(i+1, 1) = file(i) + 1;
23
24         if ~mod(i, only_number)
25             file(i, 2) = file(i) + 1; %pump only
26             file(i, 3) = file(i) + 2; %probe only
27         end
28         if ~mod(temp_var, only_number)
29             file(i+1) = file(i) + 3; %continue pump/probe files
30         end
31     end
32
33     file = file(1:end-1, :);
34
35     %for excel
36     names = {'time / ps', 'Pump Probe', 'Pump only', 'Probe only'};
37     excel_data = [time, file];
38     sheet = 1;
39     xlRange = 'A2';
40     xlRange1 = 'A1';
41
42     cd('C:\Users\labor\Desktop') %where you want to save the data
```

```
43     xlswrite(filename,excel_data,sheet,xlRange);
44     xlswrite(filename,names,sheet,xlRange1);
45     cd(currpath)
46 end
```

E Detailed Measurement Routine

In this section the measurement process for acetone is listed. This is a step-by-step instruction.

- ☐ set OPA wavelength and optimize stabilization (see chapter 2.2.3)
- ☐ take OPA and SHG spectra
- ☐ switch to xenon gas to measure cross-correlation
 - turn off MCP
 - close needle valve (care: xenon bottle has 50 bar)
 - mount off acetone reservoir
 - mount on membrane pump and turn it on
 - open valve to pump
 - bake out with heat gun (some minutes) and wait to cool down
 - close valve to pump and turn pump off
 - open xenon valve and carefully let xenon flow in (care: if the pressure raises too fast, continue closing the dosing valve)
 - set pressure with dosing valve to $2 \cdot 10^{-6}$ mbar and wait till it stays constant
 - turn off (hot cathode)- pressure sensor
 - apply 2 kV for ion measurement
 - turn on MCP
 - rotate wire grid polarizer to 120° (maximum output power)
 - set SHG-only counts to 300 (Gate A: 10.5 μ s delay, 2 μ s width)
 - position the stage on temporal overlap and optimize signal with spatial overlap (with beam profiler). Attention: Changing the wavelength can also change the overlap a bit. Then scan the stage roughly using 'Timescancount2gates'.
 - if overlap is found make a fine scan: 5 fs step size, 5 s integration time
 - check if cross correlation is o.k. (70-80 fs FWHM), else readjust prism compressor (like in chapter 2.4.1)
- ☐ switch back to acetone
 - block out laser, turn 2 kV off

- close needle valve
- close xenon bottle and xenon valve
- turn on pump and open pump valve to pump out the remaining xenon
- screw pump off and screw on acetone (maybe acetone has to be refilled)
- open needle valve and set pressure to $4 \cdot 10^{-6}$ mbar (attention: it can take very long till the pressure stays constant, check every 10 min)
- turn on repeller voltage and coil current for e^- measurement

□ Acetone time scan

- set OPA-only counts: 1000 cps (use Gate B for e^-)
- set SHG-only counts: 500 cps
- check contrast of pump-only & probe-only vs. pump/probe
- measure powers of both paths
- use 'Timescancount2gates' to see roughly if the curve of the time scan looks o.k.
- make an PE spectrum at 300 fs (check, if the characteristic peaks of the 3p states) are visible, by using 'abs_move(TimeToPos(0.3,pos0))'. Pos0 is determined from xenon measurement (true time zero point)
- close plastic cover to increase stability
- test 'PPShutter' separately; Commands: PPShutter 'U/R/O/P')
- block out laser; turn coil off; check pressure again ($4e-6$ mbar)
- if everything is o.k. unblock laser and turn coil current on
- start time scan with pumpprobe_various_dt and write down first filename
- use create_eiTOFname to make an automatic excel list with all filenames which can directly be included in OneNote
- check value of counts sometimes during long time measurements (to see if power / beams are drifting)

Bibliography

- [1] A. Zewail, The Nobel Prize in Chemistry 1999, **1999**.
- [2] A. Stolow, A. E. Bragg, D. M. Neumark, *Chemical reviews* **2004**, *104*, 1719–1758.
- [3] I. Hertel, W. Radloff, *Reports on Progress in Physics* **2006**, *69*, 1897.
- [4] A. Shastri, P. J. Singh, *Journal of Quantitative Spectroscopy and Radiative Transfer* **2016**, *173*, 92–105.
- [5] M. Hachey, F. Grein, The Role of Rydberg States in Spectroscopy and Photochemistry Low and High Rydberg States, **1999**.
- [6] E. W.-G. Diau, C. Kötting, A. H. Zewail, *ChemPhysChem* **2001**, *2*, 273–293.
- [7] D. ter Steege, A. Wirtz, W. Buma, *The Journal of chemical physics* **2002**, *116*, 547–560.
- [8] M. Nobre et al., *Physical Chemistry Chemical Physics* **2008**, *10*, 550–560.
- [9] R. McDiarmid, A. Sabljic, *The Journal of chemical physics* **1988**, *89*, 6086–6095.
- [10] P. Maierhofer, M. Bainschab, B. Thaler, P. Heim, W. E. Ernst, M. Koch, *The Journal of Physical Chemistry A* **2016**, *120*, 6418–6423.
- [11] M. Koch, P. Heim, B. Thaler, M. Kitzler, W. E. Ernst, *Journal of Physics B: Atomic Molecular and Optical Physics* **2017**, *50*, 125102.
- [12] M. Koch, B. Thaler, P. Heim, W. E. Ernst, *The Journal of Physical Chemistry A* **2017**, *121*, 6398–6404.
- [13] N. Rusteika, K. B. Møller, T. I. Sølling, *Chemical Physics Letters* **2008**, *461*, 193–197.
- [14] O. Hüter, F. Temps, *The Journal of Chemical Physics* **2016**, *145*, 214312.
- [15] D. E. Couch, H. C. Kapteyn, M. M. Murnane, W. K. Peters, *The Journal of Physical Chemistry A* **2017**, *121*, 2361–2366.

-
- [16] T. I. Sølling, E. W.-G. Diau, C. Kötting, S. De Feyter, A. H. Zewail, *ChemPhysChem* **2002**, *3*, 79–97.
- [17] P. Farmanara, V. Stert, W. Radloff, *Chemical Physics Letters* **2000**, *320*, 697–702.
- [18] W. Von der Linden, V. Dose, U. Von Toussaint, *Bayesian probability theory: applications in the physical sciences*, Cambridge University Press, **2014**.
- [19] S. Mai, P. Marquetand, L. González, *International Journal of Quantum Chemistry* **2015**, *115*, 1215–1231.
- [20] S. Ranftl, Master’s thesis, Institute of Experimental Physics, **2017**.
- [21] P. Maierhofer, Master’s thesis, Institute of Experimental Physics, **2016**.
- [22] M. Bainschab, Master’s thesis, Institute of Experimental Physics, **2016**.
- [23] B. Thaler, Master’s thesis, Institute of Experimental Physics, **2017**.
- [24] P. Heim, Master’s thesis, Institute of Experimental Physics, **2017**.
- [25] L. Treiber, Master’s thesis, Institute of Experimental Physics, **2018**.
- [26] R. Photonics, Phase-matching Bandwidth, https://www.rp-photonics.com/phase_matching_bandwidth.html.
- [27] M. Koch, T. J. Wolf, J. Grilj, E. Sistrunk, M. Gühr, *Journal of Electron Spectroscopy and Related Phenomena* **2014**, *197*, 22–29.
- [28] L. Conversion, Traveling-wave Optical Parametric Amplifier of White-light Continuum, User’s manual.
- [29] Technology, A. C. N. Corporation, Application Note, Prism Compressor for Ultra-short Laser Pulses.
- [30] F. Applloner, Master’s thesis, Institute of Experimental Physics, **2015**.
- [31] D. S. Foundation, Writing your first Django app, part 1, <https://docs.djangoproject.com/en/2.0/intro/tutorial01/>.
- [32] R. P. Foundation, GPIO, <https://www.raspberrypi.org/documentation/usage/gpio/README.md>.
- [33] MobaXterm, MobaXterm, <https://mobaxterm.mobatek.net/>.
- [34] Homepage Oversight, <https://fexphrpifslab.tugraz.at/oversight/>.
- [35] HeSurfer wiki, <https://heliumstreuung.tugraz.at/doku.php?id=getsslcert>.
- [36] A. A. P. und Elektronik GmbH, Online Calculator, <https://www.ape-berlin.de/en/calculator/>.

- [37] R. Trebino, *Frequency-resolved optical gating: the measurement of ultrashort laser pulses*, Springer Science & Business Media, **2012**.
- [38] N. Corporation, FemtoOptics Mounted Dispersion Wedge, 20x30 mm, 0.2 mm thick, Uncoated, <https://www.newport.com/p/23RQ12-02-M>.
- [39] Adafruit, MCP3008, <https://learn.adafruit.com/raspberry-pi-analog-to-digital-converters/mcp3008>.
- [40] P. Vacuum, TPG 361, TPG 362; Mnemonics and Pfeiffer Vacuum Protocol for Single- and Dual-Channel Measurement and Control Units for ActiveLine Gauges, Communication Protocoll, **2015**, Chapter 1.

List of Figures

1.1	The basic principle for a pump-probe experiment.	2
1.2	Sketch of acetone, showing the C_{2v} symmetry around the z-axis (dashed line).	4
2.1	The basic setup for the gas phase experiment and He_N -droplets. This setup includes the Legend Laser System, pump and probe path, time of flight spectrometer and analysis tools.	10
2.2	The whole optical setup with all important components: OPA, prism compressor, wire grid polarizer, delay stages and beam profiler.	11
2.3	PE spectrum using a $1000\mu m$ crystal in the probe path. Measurement date: 19.10.2017, eiTOF number: 4849	14
2.4	Three single Gaussian fits and FWHM of each fit. Green: $3p_x$, red: $3p_y$, blue: $3p_z$	15
2.5	Basic principle of our time of flight spectrometer: pump and probe pulses are focused into the measurement chamber where e^- or i^+ are pushed into the flight tube using different repeller voltages.	16
2.6	Beam path through the OPA, chosen from the manual [28].	19
2.7	Reduction of the complex system in figure 2.6 to an easier understandable block diagram to demonstrates how 333 nm is created.	19
2.8	Adjustment of the OPA: Figure a) shows all its important components. Red line: incoming beam from the Legend laser. Blue circles: Spots which should be checked in the first in-coupling routine. Green circles: The four components which are used when maximizing output power and stability. Figure b) shows where a alignment aperture is placed to check if the beam goes through the OPA correctly.	20

2.9	The OPA security box where a photo resistor is used to measure a reflex (blue arrow) from the WGP. The electronics of the box is build in the red box. LEDs indicate the trigger level and intensity of the reflex. Button 1 is used to open shutter 1 by hand.	24
2.10	Typical electron time scan with indium. The left figure shows the temporal overlap in time in ps, the right figure indicates the position of the overlap on stage 2 in mm. Pump wavelength: 375 nm, probe wavelength: 420 nm. Measurement date: 28.07.2017	25
2.11	Working principle of a prism compressor: The prisms are arranged in a configuration that the red part of the light is delayed by having a longer optical path through the prisms compared to the blue part. The dashed line indicates the mirror point. The picture is taken from the Newport manual [29].	27
2.12	A folded geometry prism compressor as used in our laboratory.	28
2.13	Prism compressor of our laboratory. Figure a) includes all its components. Figure b) shows the beam path. The dashed line is the reflected beam after the mirror and goes under the incoming beam. The power is set with a wire grid polarizer.	29
2.14	Flow chart how our homepage works in principle.	31
2.15	Restart oversight.	32
2.16	Restart nginx.	32
2.17	Homepage oversight in general.	33
2.18	Administration side where sensors can be added.	33
2.19	How to a add sensor.	34
2.20	Example for a pressure readout.	34
2.21	Server certificate.	35
2.22	Example for csr.	36
3.1	PE spectra for different repeller voltags. The improvement of the energy resolution is clearly observable for higher positive repeller voltages. At some voltage the signal drops. Pump wavelength: 336 nm, probe wavelength: 401 nm. Measurement date: 08.02.2018	39
3.2	Comparison of two peaks with 0.0 V and 1.1 V repeller voltage. Orange spectrum: left peak: $3p_x$, middle peak: $3p_y$, right peak: $3p_z$	40
3.3	Total counts over repeller voltage. At some point the electrons do not have enough kinetic energy to hit the detector which will result in a drop of the signal.	40

3.4	Ionization potential for xenon. Three pump photon and one probe photons are used to ionize the atom. Pump wavelength: 333 nm , probe wavelength: 405 nm	42
3.5	Example of a bad cross-correlation. The temporal resolution is about 100 fs. Pump wavelength: 333 nm , probe wavelength: 405 nm. Measurement date: 04.01.2018, time scan number: 1126	43
3.6	Better cross-correlation with a width of 77 fs. This cross-correlation is used in our experiment to make vibronic coupling visible. Pump wavelength: 333 nm, probe wavelength: 405 nm. Measurement date: 04.01.2018, time scan number: 1130	44
4.1	The potential energy of different states in acetone in the C=O stretch reaction coordinate. The green, red and blue values on the y-axis indicate the synchrotron measurements [8]. The black values are our chosen wavelengths. The black dashed line shows the excitation energy in the current experiment. The OPA pulse has a bandwidth of 80 meV.	48
4.2	Evaluation of the PE peaks by fitting a combination of three Gaussian peaks into it. The black curve is the PE spectrum including the three peaks of the three states. The cyan curve indicates the fit model, in contrast, green, red and blue curves are the single Gaussian fits for every peak. Measurement date: 24.10.2017	50
4.3	PE spectra for different time delays: a) 0 fs, b) 130 fs, c) 300 fs, d) 500 fs. Measurement date: 24.10.2017	51
4.4	Time scan with 333 nm and >100 fs temporal resolution. The three different curves indicate the 3p states: green: 3p _x , red: 3p _y , blue: 3p _z . Black lines: PE spectra at different time delays for figure 4.3 Measurement date: 24.10.2017, eiTOF files: 5149-5243	53
4.5	Final high resolution time scan at 333 nm and 77 fs temporal resolution. The time constants are fitted using an exponential fit model. Measurement date: 09.01.2018, eiTOF: 7313-7405	54
4.6	Zoomed into overlap region from figure 4.5. In this figure the shift of the maxima of 3p _x compared to the other states is visible. In addition the cross-correlation signal with xenon (black curve) is printed to indicate the time zero point of the cross-correlation. Measurement date: 09.01.2018, eiTOF files: 7313-7405	55
4.7	Basic example of vibronic coupling. The electronic state and vibrational state have their own different symmetries but in combination the whole symmetry can change.	56

5.1	Pin assignment of Pi 2 Model B v1.1 [32].	60
5.2	Pin assignment of the ADC MCP3008 [39].	60
5.3	How to run simpletest.py in the Python terminal.	61
5.4	The OPA wavelength ranges, extracted from the manual [28].	67

List of Tables

1.1	Character table of the C_{2V} pointgroup $A_1, A_2, B_1, B_2 \cdots$ symmetries E \cdots identity $C_2(z) \cdots$ rotation about 180° around z-axis $\sigma_v(xz / yz) \cdots$ reflection at plane in xz or yz	4
1.2	Product table of the C_{2V} pointgroup $A_1, A_2, B_1, B_2 \cdots$ symmetries	5
2.1	List of the SHG crystals in the laboratory $l \cdots$ length of the crystal $\sigma_{FWHM} \cdots$ spectral width (full width half maximum) of the crystal $E_{SHG} \cdots$ energy resolution of the SHG crystal $\tau_{TL} \cdots$ transformlimit $\Delta E_{res, 1} \cdots$ en- ergy resolution of the setup for different SHG crystals of length l	14
2.2	Dichroic mirrors which can be build in the OPA to set the wavelength range $\lambda \cdots$ wavelength	21
3.1	Theoretical cross-correlations $l \cdots$ length of the crystal $\tau_{SHG} \cdots$ transform- limit of SHG crystal $\tau_{OPA} \cdots$ transformlimit of OPA $\tau_{theor} \cdots$ theoretical transform limited cross-correlation	45
4.1	Calculated time constants from theory State \cdots name of the excited state $\tau \cdots$ time constant of the state Err \cdots error of the time constant Sym \cdots symmetry of the states $E \cdots$ energy level of each state	49
4.2	Calculated and measured time constants State \cdots name of the excited state $\tau_{theory} \cdots$ theoretical time constants $\tau_{fit} \cdots$ fitted time constants Sym \cdots symmetry of the states	54
4.3	Product table of C_{2V} pointgroup $A_1, A_2, B_1, B_2 \cdots$ symmetries of the electronic state $a_1, a_2, b_1, b_2 \cdots$ symmetries of the vibrational state	56
5.1	Pins of the Raspberry Pi	59
5.2	Communication commands	65

Danksagung

Zum Abschluss meiner Masterarbeit möchte ich mich bei den vielen Menschen bedanken, die mich während meines Studiums begleitet haben.

Ein großes Dankeschön gilt meinem Betreuer Assoc.Prof. Dipl.-Ing. Dr.techn. Markus Koch. Durch die Chance in deiner Forschungsgruppe mitarbeiten zu dürfen habe ich mich in meinem letzten Studienjahr fachlich und persönlich um einiges weiterentwickelt. Deine exzellente Betreuung, bei der du immer bemüht bist auch ein gutes persönliches Verhältnis zu schaffen, ist schwer zu übertreffen. Du findest stets das richtige Maß, wie weit du jemanden fordern kannst. Deine ruhige Art bei unseren fachlichen Diskussionen ist einer der Hauptgründe weshalb das Arbeitsklima innerhalb unserer Gruppe so entspannt ist. Während der letzten Monate hast du mir nicht nur neue Arbeitsabläufe gezeigt ("Da sieht man mal wieder wie wichtig es ist Ergebnisse zu reproduzieren."), ich habe durch dich auch gelernt, wie man (physikalische) Probleme richtig hinterfragt und löst ("Da sieht man ganz klar eine Oszillation.").

Des Weiteren möchte ich mich bei dem Leiter des Instituts für Experimentalphysik Univ.-Prof. Dipl.-Phys. Dr.rer.nat. Wolfgang E. Ernst für die Möglichkeit bedanken meine Masterarbeit hier an diesem Institut verfassen zu können.

Bei meinem Laborpartner Sascha Ranftl bedanke ich mich für die angenehme Zeit und die musikalische Verwöhnung (Gigi-Donnerstag). Wir haben schon letzten Sommer Geschichte geschrieben und physikalische Effekte beobachtet, die uns damals niemand glauben wollte.

Besonders gedankt sei an dieser Stelle Bernhard Thaler, sowie Matlab- und Boulder Coach Pascal Heim, die bei jedem erdenklichen Problem immer mit Rat und Tat zur Seite standen. Danke, für die viele Geduld, sei es beim Einschulen an unserer Apparatur oder bei den vielen detaillierten Diskussionen.

Für die gute Zusammenarbeit im Labor und der guten Stimmung in unserem Büro bedanke ich mich ebenfalls bei Miriam Meyer, Leonhard Treiber und Werner Kleinsasser. Hoffentlich habt ihr weiterhin noch viel Spaß mit Mr. Femto.

Bei allen Mitarbeitern der Forschungsgruppen unseres Instituts bedanke ich mich für den Toasty-Tuesday, Noodle-Wednesday, dem Pub-Quiz im North und den wichtigen Kaffeepausen.

Größter Dank gebührt meinen anfänglichen Unikollegen, die inzwischen zu meinen guten Freunden geworden sind: Bernhard Thaler, Andreas Jeindl, Lukas Hörmann, Sascha Ranftl und Sarah Dörschlag. Ohne euch wäre mein Studium sicherlich nicht so lustig und reibungslos verlaufen. Danke, dass ihr mich immer motiviert habt. Ein bisschen werde ich das Rechnen der Übungszettel und die nächtlichen Lerneinheiten mit euch vermissen.

Für die Gestaltung diverser Freizeitaktivitäten bedanke ich mich neben meinen oben erwähnten Unifreunden vor allem bei Mario Poschner. Hallo Mario, während ich diese Zeilen verfasse, bist du wahrscheinlich gerade auf den Weg ins Music-House. Keine Angst, wir sehen uns gleich.

An dieser Stelle bedanke ich mich ebenfalls bei meiner Pub-Gang Lukas Wielandner, Ralf Lehner, Fabian Lindner, Markus Koller und Jonas Sieff.

Wenn ich zurück nach Kärnten fahre ist es jedes Mal schön meine langjährigen Freunde Christian, Carina, Anna, Michael, Anna und Tina zu treffen. Vielen Dank, dass ihr mich immer wieder auf die wichtigen Dinge im Leben aufmerksam macht. Wir kennen uns alle jetzt schon so lange und es freut mich, dass ich mich immer auf euch verlassen kann.

Vielen Dank an Alfred Nowak, einem Menschen, der mich sehr inspiriert und der mitunter auch ein Grund ist, warum ich Physik studiert habe.

Abschließend möchte ich noch schreiben, dass mein ganzes Studienleben nicht so entspannt möglich gewesen wäre, hätte ich nicht seit jeher den absoluten Rückhalt meiner Familie erfahren. Meinen Eltern Andrea und Dietmar, meiner Oma Erika, meiner Tante Rosi, sowie meinem Onkel Gerhard und dessen Frau Evelin danke ich nicht nur für die finanzielle und seelische Unterstützung, ihr habt immer an mich geglaubt, mich immer meinen eigenen Weg gehen lassen und meine persönlichen Entscheidungen nie in Frage gestellt. Ein größeres Glück kann man nicht haben.

Graz, Mai 2018

Stefan Cesnik

